International Journal of Innovative Computing, Information and Control
Volume **20**, Number **6**, December **2024**

ICIC International ©2024 ISSN 1349-4198
pp. **1683–1716**

A NOVEL THIRTEEN-DEGREE-OF-FREEDOM MODEL EMPLOYING THE NEWMARK METHOD WITH VARIED WHEEL INPUTS FOR OPTIMIZING VIBRATION AND COMFORT IN WHEELCHAIR-OCCUPANT SYSTEMS

Pongtep Weerapong[1,*], Kreetha Kaewkongtham[1], Narapong Chuaychai[1]
Suppharerk Kathammanee[1], Weeraphol Pansrinual[1]
Kridtharit Thongsin[2], Nghia Thi Mai[3], Md Abdus Samad Kamal[4]
Iwanori Murakami[4] and Kou Yamada[4]

[1]Faculty of Industrial Technology
Nakhon Si Thammarat Rajabhat University
1 M.4, Tha Ngio, Maung Nakhon Si Thammarat, Nakhon Si Thammarat 80280, Thailand
{ kreetha_kae; narapong_cho; suppharerk_kat; weeraphol_pan }@nstru.ac.th
*Corresponding author: pongtap_wee@nstru.ac.th

[2]Faculty of Engineering and Industrial Technology
Bansomdejchaopraya Rajabhat University
1061 S.Itsaraphap 15, Itsaraphap Road, Hiranruchi, Thonburi, Bangkok 10600, Thailand
kridtharit.th@bsru.ac.th

[3]Faculty of Electronics Engineering 1
Posts and Telecommunications Institute of Technology
122 Hoang Quoc Viet Road, Cau Giay District, Hanoi 11355, Vietnam
nghiamt@ptit.edu.vn

[4]Division of Mechanical Science and Technology
Gunma University
1-5-1 Tenjincho, Kiryu 376-8515, Japan
{ maskamal; murakami; yamada }@gunma-u.ac.jp

Received March 2024; revised July 2024

Abstract. *Wheelchair users encounter vertical vibrations that can impinge on their comfort and well-being. This study introduces and corroborates a sophisticated 13-DOF model for a wheelchair-occupant system, accounting for unique input excitations at each wheel. Employing the Newmark method and Fourier analysis, the model scrutinizes vibration responses within time and frequency spectrums. Experimental data substantiate the model, evidencing an impressive goodness-of-fit. Furthermore, the investigation delves into the biodynamic reactions of wheelchair users, exploring how cushion attributes influence vibration dynamics. It is determined that seat cushions devoid of foam significantly augment vibration intensity throughout all body regions. The model emerges as an instrumental resource for the conceptualization and evaluation of wheelchair cushions, enhancing both comfort and security. This paper propels the understanding of wheelchair-occupant interactions, underscoring their significance for user health and functional performance. The findings render crucial contributions to wheelchair design and occupant safety.*

Keywords: Wheelchair-occupant system, Vertical vibration transmission, Newmark method, Biodynamic responses, Ride comfort and safety

DOI: 10.24507/ijicic.20.06.1683

1. **Introduction.** Vibrations profoundly impact human health and performance, especially in the context of wheelchair use, where factors such as road surface conditions, driving speeds, wheelchair components and occupant postures amplify their effects. Various studies have identified several critical gaps within this domain. For instance, Toro-Hernández et al. [1] highlighted a deficiency in wheelchair provision knowledge among Colombian occupational therapy students; Geers et al. [2] emphasized the need for custom head supports in wheelchairs; and Lariviere et al. [3] examined factors influencing vibration transmission in manual wheelchairs. ISO 8608:2016 [4] set standards for reporting vertical road profile data and research by Agostinacchio et al. [5] and Quadros et al. [6] indicated that road surface degradation significantly increases vibration levels. Vibration exposure has numerous adverse effects on comfort, safety and health, including motion sickness, spinal deformities, pressure ulcers, muscle fatigue and lower back pain [7], with Wolf et al. [8] underscoring these severe health risks and stressing the need for effective vibration mitigation strategies. Additional research, such as the work by Waga et al. [9], explored the role of different materials in vibration transmission, offering critical insights for designing wheelchairs that minimize vibrations. Garcia-Mendez et al. [10] advocated for enhancing wheelchair designs to mitigate health risks associated with vibration exposure, proposing a holistic design approach. Duvall et al. [11, 12] set standards for surface roughness in wheelchair pathways to reduce vibration exposure, while Hischke and Reiser [13] evaluated the effectiveness of rear-wheel suspension systems in controlled environments, noting the need for further research to assess their real-world effectiveness. Adam et al. [14] analyzed the effect of posture on vibration transmissibility, highlighting its importance in wheelchair design.

Previous studies by Brown et al. [15] and Weerapong et al. [16] employed advanced modeling and simulations to predict how vibrations affect wheelchair users under various conditions. Garcia-Mendez et al. [17] focused on whole-body vibration exposure in manual wheelchair users, highlighting the role of different wheelchair components. Nadalin et al. [18] linked occupational whole-body vibration exposure to prostate cancer, underscoring potential long-term health effects. While laboratory studies demonstrate promise, real-world testing of wheelchair components and systems remains essential to confirm their practical efficacy. Additionally, inconsistencies in research findings regarding the effectiveness of cushions and other components call for standardized testing protocols to ensure more reliable results. A comprehensive approach to wheelchair design must examine the interactions between different components to understand their collective impact on vibration transmission and user comfort. Longitudinal studies are also necessary to understand the cumulative effects of vibration exposure on health and comfort over time. This paper represents a significant advancement in the field of wheelchair dynamics, building upon and extending previous research. Earlier studies systematically quantified and analyzed the vibrational responses of standard wheelchairs and their components, identifying key characteristics such as natural frequencies, mode shapes, modal coupling, damping and the application of state-space methods to analyze vertical vibrations [19, 20, 21, 22, 23, 24, 25, 26, 27]. This paper enhances our comprehensive understanding of wheelchair dynamics, essential for advancing user comfort and safety through improved design and engineering practices. The computational model presented herein not only validates but also extends these findings, offering an in-depth assessment of the dynamic behavior of wheelchair components.

Multiple studies have emphasized the necessity for improved wheelchair designs, particularly regarding head support and vibration transmission, which significantly influence user comfort and safety [1, 2, 8, 17, 19, 28, 29]. This paper contributes to this objective

by providing an advanced tool for evaluating the performance of various wheelchair components and their interactions. Furthermore, this research aligns with studies that have examined various factors influencing wheelchair vibrations, including material properties, analytical methods, modifications and control strategies [9, 30, 31, 32]. The computational model enables a comprehensive examination of these factors and their impacts, fostering a deeper understanding of wheelchair dynamics. By illustrating the model's applicability and validity for specific systems under vertical vibrations with distinct input excitations for each wheel, this paper offers valuable insights into system behavior, vibration transmission to different body segments and the effects of factors such as cushion type, input amplitude and input frequency [12, 16, 33]. Ultimately, this paper aims to spark interest and innovation within the field, contributing to an improved quality of life for wheelchair users. While this research provides valuable insights into the biodynamic responses of wheelchair users exposed to vertical vibrations, several limitations must be considered. One notable shortcoming is the focus on a single type of wheelchair and a specific foam-based cushion design. Future research should explore a wider range of wheelchair types and cushioning materials to generalize findings. Additionally, the emphasis on vertical vibratory inputs may overlook real-world conditions where multi-directional vibrations are prevalent. Comprehensive studies that integrate horizontal and lateral vibrations would offer a more holistic view of vibrational impacts on wheelchair users. Furthermore, the study primarily employs a composite model with minimal response parameters, which, while useful, may not capture the full complexities of human body dynamics under vibrational stress. Enhanced models incorporating more extensive physiological and biomechanical parameters could provide deeper insights and more accurate predictions of vibrational impacts [20, 34, 35].

To bolster and contextualize the findings of this paper, it is essential to review recent studies in the field. Lariviere et al. conducted a systematic review on vibration transmission during manual wheelchair propulsion, emphasizing the critical need for effective vibration attenuation to enhance user comfort and health [19]. Their findings align with our research, reinforcing the importance of addressing vibration transmission in wheelchair design. Additionally, Weerapong et al. performed a modal analysis on a wheelchair-occupant model with a foam-based seat cushion, similar to our study [20]. Their work corroborates our findings on the efficacy of foam-based materials in vibration reduction but also points out the necessity of multi-modal approaches to comprehensively capture complex vibrational behaviors. Further, Lariviere et al. conducted experimental modal analyses of standard wheelchairs, providing insights into the modal characteristics of manual wheelchairs [21, 22]. These studies revealed the intricate vibratory interactions between wheelchair components, highlighting areas for potential improvements in wheelchair design. Contributions by Nangolo et al. and Schwochow and Jelcic, who conducted combined numerical and modal analyses to study vibrational responses in railway vehicles and aeroelastic applications respectively, provide methodological insights that, although not directly related to wheelchairs, could inform advanced analytical techniques for studying wheelchair vibrations [23, 24]. Miao et al. discussed sub-cycling methods for flexible multi-body dynamics, offering potential applications for analyzing complex vibrational systems in wheelchairs [25]. Yuan et al. employed operational modal identification techniques for precision machinery, which could be adapted for detailed vibrational analysis in wheelchair systems [26]. Weerapong et al. further expanded on vertical vibration behavior in wheelchair-occupant systems using a composite model, providing advanced analytical frameworks that align well with our research objectives [27].

This paper aims to develop and validate an innovative 13-degree-of-freedom (13-DOF) model of a wheelchair-occupant system, offering a comprehensive framework for examining vibration transmissibility from the wheelchair to various parts of the occupant's body. This model integrates a foam-based seat cushion and suspension system, with parameters carefully selected from existing literature and experimental data. These selection criteria ensure accuracy and relevance, incorporating material properties such as density and damping coefficients derived from experimental studies on foam-based cushions and suspension components, as well as anthropometric data sourced from biomechanical research on human body dynamics under vibrational forces. To solve the linear equations of motion within this framework effectively, the Newmark method is utilized, enabling iterative updates of displacement, velocity and acceleration for each degree of freedom at every time step. Complementing this method, Fourier transformation is employed to analyze signals in both time and frequency domains. This robust and comprehensive approach allows the model to handle a wide range of input excitations, providing profound insights into system behavior and the transmission of vibrations to different body segments [20, 34, 35].

The model's relevance and rigor are further underscored by its adherence to International Standards Organization (ISO) 2631-1:1997 standards, which provide criteria for evaluating human exposure to whole-body vibration. By comparing the vibration transmissibility of all body parts against ISO exposure limit curves – which indicate acceptable levels of vibration for different exposure durations – this study provides a detailed analysis of acceleration responses across anatomical regions during wheelchair mobility.

To address the existing gap, this paper develops and validates a 13-degree-of-freedom (13-DOF) model capable of capturing and predicting the complex dynamic responses of wheelchair-occupant systems under varying vertical vibration scenarios. The validation of this model enhances our understanding of the intricate interactions between different body regions and wheelchair components, paving the way for innovations in wheelchair design. By investigating specific biodynamic reactions of wheelchair users and cushion characteristics, this study provides critical insights into optimizing seat cushion designs. This work aims to significantly enhance user comfort and mitigate health risks, aiding the development of next-generation wheelchairs optimized for both comfort and safety.

The structure of this paper is as follows. Section 2 reviews the challenges and methods of analyzing the dynamics of wheelchair-occupant systems using free-body diagrams (FBDs) and ordinary differential equations. Section 3 explains the system modeling and lumped mechanical system dynamics for vibration analysis. Section 4 presents the time-domain approach using the Newmark algorithm and Fourier transform. Section 5 provides a numerical example illustrating the equations of motion that describe the dynamic behavior of the 13-degree-of-freedom (13-DOF) wheelchair-occupant model. The Fourier transform is applied to shift equations derived from the Newmark method to the frequency domain. The equations of motion (EOMs) of the multi-degree-of-freedom (MDOF) system are solved using the finite difference (FD) method, focusing on the steady-state response under various input excitations. Section 6 validates the 13-DOF model with varied input excitations, comparing results with experimental data and examining the effects of different factors on dynamic response, vibration transmission and seat transmissibility using a goodness-of-fit approach. Section 7 concludes the paper and suggests directions for future research.

2. **Vibrational Exposure and Multibody Analysis of the Wheelchair-Occupant System.**

Analyzing the dynamics of wheelchair-occupant systems presents formidable challenges due to their intricate complexity and diagnostic intricacies. However, by representing the occupant and wheelchair as free-body diagrams (FBDs), we can more efficiently

solve a linear system of ordinary differential equations in the 13-DOF model. We use FBDs to establish equilibrium equations for each component, facilitating the derivation of the motion equations. From a mechanical standpoint, we analyze the system. It consists of 13 masses, 17 springs and 17 dampers. We consider inertial forces, stiffness forces and damping forces.

The inter-connective reaction forces generated by stiffness and damping are also accounted for. Each component is depicted by an FBD and the direction of forces is determined by applying Newton's third law of motion. For instance, when considering masses m_{10}, m_{11}, m_{12} and m_{13} relative to the ground, the compressed rubber tires generate stiffness and damping forces that result in an upward thrust on the wheelchair-frame and wheels along the y-axis. The inertia force of masses opposes positional changes through their inertial force. Gravitational force and static displacement of each mass are not considered in the FBDs, as they are in motion [45].

2.1. **Model development of the wheelchair-occupant system.** Our objective is to examine how a person seated in a wheelchair responds to vibration during operation. The seat cushion provides support to the lower body. The upper segment lacks a backrest. The only external impulse transmitted to the human body is a sinusoidal force input. It is generated by the stiffness and damping forces from the wheelchair wheels on the ground. We disregard external forces acting on the foot support of the wheelchair, as they have minimal impact on vibration and primarily affect the trunk region of the body. To thoroughly investigate this system, we propose a wheelchair-occupant model illustrated in Figures 1 and 2. Using the lumped-parameter model, we analyze how the system responds to vibration under steady-state conditions within the low frequency range of 0.5 to 20 [Hz]. The 13 block composite model, known as a 13-DOF model, comprises a wheelchair model and a human occupant model interconnected through stiffness and damping constants.

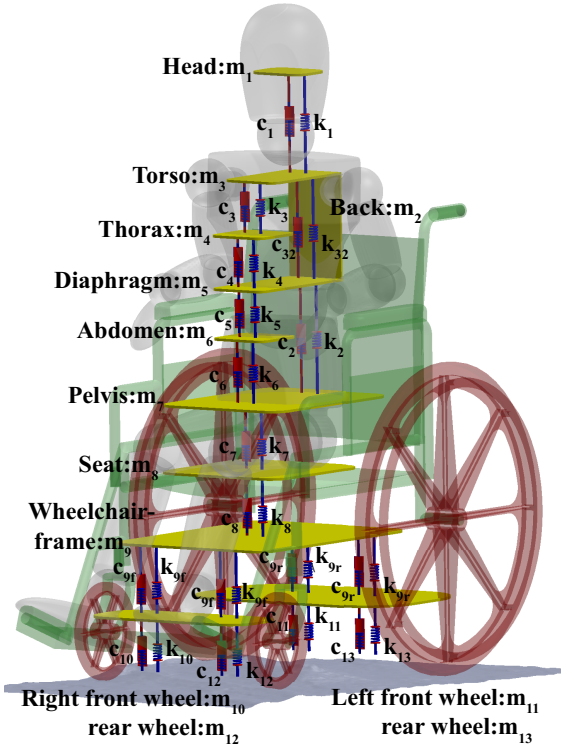

FIGURE 1. Thirteen lumped-mass models of a wheelchair-occupant system

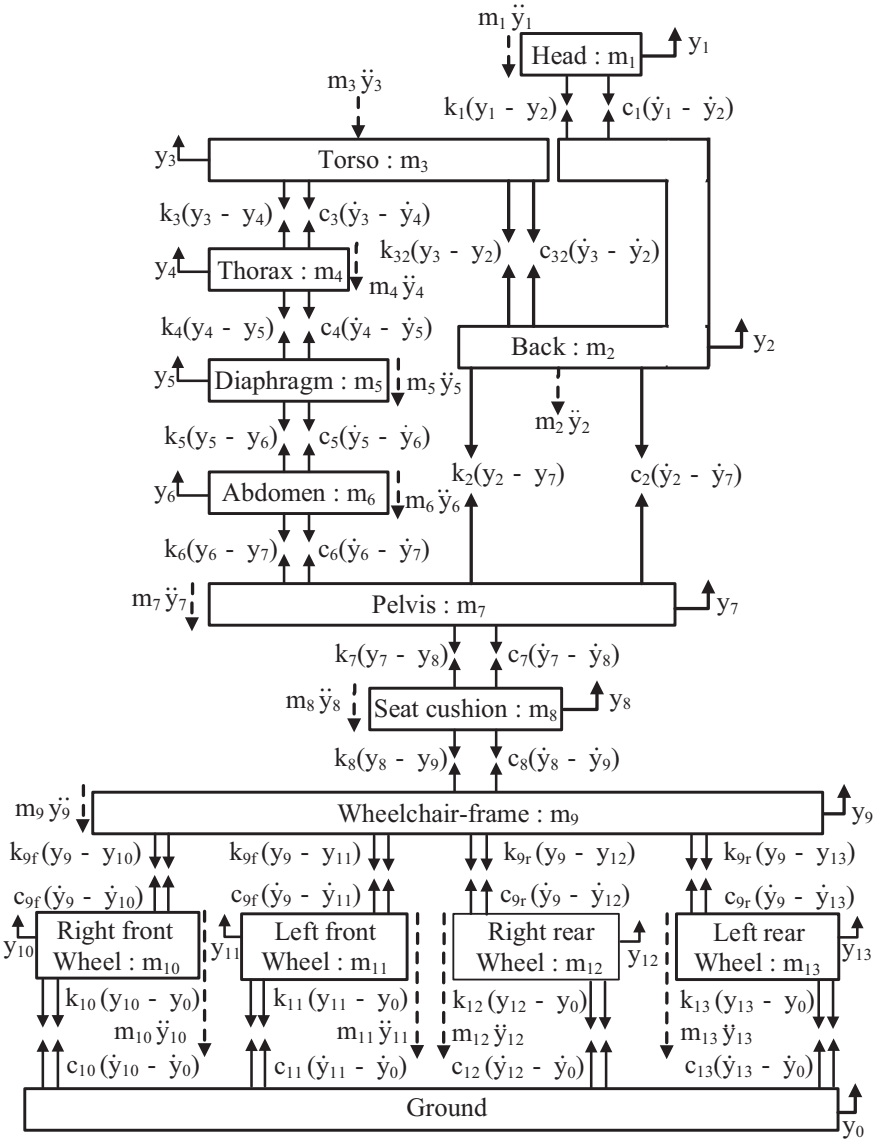

FIGURE 2. The lumped-parameter model for the wheelchair-occupant system consists of free body diagrams for each component of the system.

The blocks represent masses denoted as m_i with $(i = 1, 2, \ldots, 13)$, corresponding to various body parts such as the wheelchair-frame and wheels, seat, pelvis, head and others. We establish connections between these blocks using stiffness and damping constants denoted as k_i and c_i, respectively. Detailed parameter values for the body parts and wheelchair parts can be found in Tables 1 and 2, respectively. Further analysis details are discussed in subsequent sections, utilizing the 2-D sagittal plane perspective depicted in Figures 1 and 2.

2.2. **Comprehensive criteria for parameter selection and determination methods.** The proposed model must meticulously outline criteria for selecting parameters and the methods for determining these parameters, grounded in both experimental evidence and scholarly research.

2.2.1. *Criteria for selecting parameters.* i) Physiological Accuracy: Parameters should accurately reflect human biomechanical properties to replicate authentic responses to

TABLE 1. Biodynamic model parameters and their values

Mass[M] [kg]	Damping constant[C] [N/m/sec]	Spring constant[K] [N/m]
$m_7 = 27.7$	$c_7 = 378$	$k_7 = 25500$
$m_6 = 6.02$	$c_6 = 298$	$k_6 = 894.1$
$m_5 = 0.46$	$c_5 = 298$	$k_5 = 894.1$
$m_4 = 1.38$	$c_4 = 298$	$k_4 = 894.1$
$m_3 = 33.33$	$c_3 = 298$	$k_3 = 894.1$
	$c_{32} = 3651$	$k_{32} = 53640$
$m_2 = 6.94$	$c_2 = 3651$	$k_2 = 53640$
$m_1 = 5.5$	$c_1 = 3651$	$k_1 = 53640$

TABLE 2. Manual wheelchair model parameters and their values

Mass[M] [kg]	Damping constant[C] [N/m/sec]	Spring constant[K] [N/m]
$m_{13} = 0.8$	$c_{13} = 250$	$k_{13} = 3000$
$m_{12} = 0.8$	$c_{12} = 250$	$k_{12} = 3000$
$m_{11} = 0.5$	$c_{11} = 250$	$k_{11} = 30000$
$m_{10} = 0.5$	$c_{10} = 250$	$k_{10} = 30000$
m_9 =15	$c_{9f} = 700$	$k_{9f} = 13400$
	$c_{9r} = 700$	$k_{9r} = 74600$
m_8 =1.5	$c_8 = 1689$	$k_8 = 183200$
Input magnitude vibration y_{10}, y_{11}, y_{12} and $y_{13} = 5$, 8, 10, 15 [mm], respectively		

The parameter values for the wheelchair-frame are denoted by the subscript 'f' for the front and 'r' for the rear.

vibrations. This includes anthropometric measurements such as body segment masses and rigidity to ensure human likeness. ii) Component-Specific Characteristics: Each wheelchair component (e.g., frame, wheels, cushions, and suspension systems) must be parameterized based on physical and mechanical properties derived from experimental data or manufacturer specifications. iii) Environmental Realism: Realistic environmental conditions, such as road surface profiles and vibration frequencies, must be incorporated to ensure the model's practical applicability.

2.2.2. *Methods for determining parameters.* Parameters in the model emerge from a combination of experimental data, literature reviews and validated computational techniques. The primary methods are as follows. i) Human Body Dynamics Parameters: Masses and Inertias: Derived from anthropometric data in biomechanics literature which provide parameters for body segments (e.g., head, torso, and limbs) as referenced in [20, 34, 35, 46]. Stiffness and Damping Coefficients: These coefficients representing the viscoelastic properties of human tissues are referenced from study by Griffin [7]. ii) Wheelchair Component Parameters: Dynamic Properties of Frame and Wheels: The mass, stiffness and damping properties of the wheelchair-frame and wheels are obtained through experimental measurements and manufacturer data [33]. Cushion Properties: Stiffness and damping of foam-based seat cushions are evaluated through material testing, as cited in studies by Garcia-Mendez [33] and Weerapong et al. [20, 34]. Suspension System Properties: Spring constants and damping coefficients are selected based on experimental studies and existing vibration reduction strategies, particularly from automotive engineering [25, 37]. iii) Environmental Inputs: Road Surface Profiles: Standardized profiles are defined as

per ISO 8608:2016 [4]. Input Vibration Frequencies and Amplitudes: Derived from real-world measurements and studies focusing on wheelchair vibrations by Wolf et al. [8] and Larivière et al. [19].

2.2.3. *Parameter determination process.* i) Collection of Experimental Data: Experimental setups are designed to replicate real-world wheelchair operational conditions. Devices such as accelerometers and force sensors measure vibration transmission and dynamic responses. ii) Estimation and Validation of Parameters: The collected data is processed using statistical and optimization techniques to estimate key parameters. Model predictions are validated through comparisons with independent experimental results. iii) Integration of Literature Data: When direct measurement is impractical, parameters from existing research are incorporated into the model. Robust parameter selection is ensured by referencing studies from various researchers [1, 6, 10].

2.3. **Simplified assumptions and model limitations.**

2.3.1. *Exclusion of gravitational effects.* In the development of the 13-DOF model of the wheelchair-occupant system, certain simplifications were employed to streamline the computational analysis while concentrating on the primary dynamic forces. One critical assumption was the exclusion of gravitational influence. For clarity, it is essential to note that gravity, expressed as a static force (mass multiplied by gravitational acceleration), exerts a uniform influence on the system and is mainly balanced by the static support structures of the wheelchair.

Given that our study focuses on the dynamic forces – transient forces resulting from rapid accelerations and decelerations – it is evident that gravitational influence has a diminished impact on the equations of motion. Consequently, gravitational effects were omitted from our dynamic analysis. This exclusion is justified as the inertial forces induced by dynamic interactions significantly overshadow the relatively constant gravitational force.

This simplification provides a more manageable analytical framework, allowing the model to emphasize the dynamic interactions and vibrational responses of the system more effectively. The validation against experimental data has demonstrated an impressive goodness-of-fit, underscoring the decision's efficacy. Although this assumption streamlines the modeling process without introducing substantial inaccuracies, it is acknowledged that real-world scenarios encompass higher complexity. Future studies may include gravitational effects to provide a more comprehensive analysis.

2.3.2. *Linear system assumption.* In developing our model, one of the core assumptions is the linear behavior of the system, despite the potential non-linearities introduced by material properties, geometric configurations and boundary conditions in real-world applications.

By assuming linearity, we achieve significant mathematical simplification, which enables the utilization of superposition principles and the application of efficient numerical methods such as the Newmark algorithm. This simplification is particularly advantageous for enhancing the tractability and computational efficiency of the model.

Additionally, for small oscillations or perturbations around the equilibrium position, most systems display behaviors that can be approximated as linear. This approach allows for both tractable analysis and sufficient precision in scenarios involving small deformations.

However, the linear approximation imposes certain limitations on the results. While it proves accurate for small displacements and forces, it may not fully capture the system's response under larger deformations or conditions where non-linear effects become

significant. Consequently, this could result in deviations from the predicted vibrational behavior in high-stress scenarios.

Furthermore, the assumption of linearity may restrict the model's generalizability to conditions that involve substantial non-linearity. Thus, incorporating non-linear elements in future iterations of the model would be critical to extending its applicability to a broader spectrum of real-world conditions, thereby enhancing its robustness and comprehensiveness.

2.4. **Vibration response of a wheelchair-occupant system as a lumped mechanical system with parameter values.** The paper presents a rigorous and original analysis of a lumped mechanical system, with a focus on the detailed modeling of the wheelchair-occupant system as shown in Figures 1 and 2. The system is modeled as a typical manual device, where the seat cushion supports the occupant's lower limbs, while the upper limbs lack support from a backrest. The paper considers only sinusoidal functions as input vibrations transmitted through the seat cushion from the springs and dampers on the wheelchair wheels. The paper ignores minor real-world vibrations transmitted through the wheelchair foot support due to their irrelevance [46]. Figures 1 and 2 provide a comprehensive cross-sectional view of the wheelchair and occupant, illustrating eleven interconnected mass blocks labeled as m_i (where $i = 1, 2, \ldots, 13$). These blocks are interconnected in pairs by springs and dampers. Notably, seven blocks representing different body parts such as the head (m_1), back (m_2), torso (m_3), thorax (m_4), diaphragm (m_5), abdomen (m_6) and pelvis (m_7) are interlinked by elastic elements, effectively capturing the resilient characteristics of the tissues between these components. The parameter values for these human tissues are derived from comprehensive studies on anatomical subsystems and are documented [46, 47] in Table 1.

In contrast, the wheelchair itself is represented as a 6-DOF system, consisting of four blocks: the seat, equipped with a cushion of negligible mass; the wheelchair-frame; the front wheels; and the rear wheels. These blocks, denoted as m_8, m_9, m_{10}, m_{11}, m_{12} and m_{13}, respectively, possess mass values listed [33, 48] in Table 2. Incorporating this multi-dimensional representation of the wheelchair-occupant system offers a synthetic and comprehensive understanding of its complex dynamics. y_{10}, y_{11}, y_{12} and y_{13} denote the road surface amplitudes, approximated as sinusoidal shapes, corresponding to wheelchair motion with different displacements for each wheel – 5, 8, 10 and 15 [mm] [6], respectively. ω is the angular frequency, defined as $\omega = 2\pi f$, where f is the frequency in the range of 0.5 to 20 [Hz]. The damping coefficients for the front wheels are $c_{10} = c_{11}$ and for the rear wheels, $c_{12} = c_{13}$. Similarly, the stiffness values for the front wheels are $k_{10} = k_{11}$ and for the rear wheels, $k_{12} = k_{13}$. The variable t represents the time period.

3. **Modeling Approach and Experimental Measurements.** A novel technique for evaluating the transmission of vertical vibrations in a wheelchair-occupant system is presented, which differs from existing literature in several key aspects. Firstly, an 13-DOF model is used, providing a more detailed representation of system dynamics than earlier models. This inclusion of additional degrees of freedom allows for a finer depiction of the occupant's vibrational response, enhancing our comprehension of transmissibility factors. The employment of Newmark's algorithm is a salient feature of this research [36, 37, 38, 39, 40, 41]. By implementing Newmark's analysis techniques, the study establishes robust and validated dynamic models, laying a strong groundwork for subsequent analyses. This methodology guarantees that the forecasted steady-state response is in close agreement with the actual measured seat transmissibility, thus improving the precision and dependability of the results. The efficacy of the analytical method used in

this research is further corroborated by comparisons with existing literature. The insights gained are instrumental for grasping the potential effects on the occupant's comfort and health and they are crucial for guiding the design of measures to alleviate excessive vibrations.

3.1. **Dynamic equilibrium framework for the 13-DOF wheelchair-occupant model.** The provided mathematical model encapsulates the dynamic equilibrium principles governing the complex interplay of mass-induced acceleration, damping-induced velocity and stiffness-driven displacement within the wheelchair-occupant system. The wheelchair-occupant system's dynamic equilibrium is characterized by a precise balance of forces and torque moments acting on each component. These include inertial forces due to mass and acceleration, damping forces due to velocity, stiffness forces due to displacement and external forces arising from road excitation. The dynamic equilibrium equations can be succinctly expressed in matrix form:

$$[M]\{\ddot{y}(t)\} + [H](\{y(t)\}, \{\dot{y}(t)\}) = \{F(t)\}. \tag{1}$$

Here, the mass matrix is represented as $[M] = [m_{ij}]$. The term $[H](y(t), \dot{y}(t))$ encompasses the internal force vector, while $\{F(t)\} = \{F_{i1}(t)\}$ signifies the external force vector. The indices $i, j \in 1, 2, \ldots, n$ denote matrix elements and n is the number of degrees of freedom (DOF) of the system. The vector $\{y(t)\} = \{y_{i1}(t)\}$ denotes the displacement of each DOF, with its first and second derivatives representing the velocity and acceleration vectors, respectively.

3.2. **Linear dynamic model.** The linear dynamic model postulates that the structure, with the internal force vector, exhibits a linear dependence on the displacement and velocity vectors. This relationship is expressed by the equation:

$$[H](\{y(t)\}, \{\dot{y}(t)\}) = [C]\{\dot{y}(t)\} + [K]\{y(t)\}. \tag{2}$$

This equation delineates the linear dynamic model, portraying a structural configuration characterized by linear stiffness and damping. Here, $[C]$ represents the damping matrix, denoted as $[c_{ij}]$ and $[K]$ symbolizes the stiffness matrix, expressed as $[k_{ij}]$. The damping matrix accounts for energy dissipation resulting from the relative motion of system components, while the stiffness matrix captures the elastic deformation and restoring forces within the system.

3.3. **Equations of motion (EOMs).** The discretized equations governing the wheelchair-occupant model with the consideration of time increments are expressed as

$$[M]\{\ddot{y}(t_n)\} + [C]\{\dot{y}(t_n)\} + [K]\{y(t_n)\} = \{F(t_n)\}, \tag{3}$$

where $[M]$ represents the mass matrix, $[C]$ denotes the damping matrix, and $[K]$ signifies the stiffness matrix. $\{y(t_n)\}$, $\{\dot{y}(t_n)\}$ and $\{\ddot{y}(t_n)\}$ are the vector of displacement, velocity and acceleration, respectively, at time t_n. $\{F(t_n)\}$ is the vector of external forces applied at time t_n. By discretizing the system at time intervals $t_0 = 0$, $t+1 = \Delta t$, $t+2 = 2\Delta t$ and so forth up to $t_n = n\Delta t$, where Δt signifies the time increment, a numerical framework is established for solving the dynamic system.

Utilizing a systematic integration methodology, the system's behavior is meticulously analyzed from one time step to the next. This method involves examining displacements, velocities and accelerations at each discrete time point and assumes linear acceleration between successive time intervals.

In the context of numerical methods like the Newmark method, the progression to the "increment $(n+1)$" at time (t_{n+1}) holds critical importance in temporal algorithms, influencing the systematic update of the system's state.

The choice of an optimal time increment, denoted as (Δt), is crucial in these equations as it dictates the precision and stability of the simulation results. By selecting a time step that aligns with the system's natural periods, the Newmark method can accurately capture dynamic responses, including resonance, transient behavior and steady-state vibrations.

Maintaining stability in the Newmark method relies heavily on selecting an appropriate time step to prevent numerical issues and ensure reliable simulation outcomes. This implicit time integration scheme benefits significantly from a well-chosen time increment, refining approximations iteratively within each time step to enhance accuracy.

In essence, the meticulous selection of the time step based on the system's inherent characteristics is fundamental for achieving precise and stable numerical simulations in engineering vibrations using the Newmark method. By adhering to these considerations, researchers and engineers can elevate the accuracy and reliability of their simulation studies, contributing valuable insights to the field of engineering vibrations.

3.4. **A critical evaluation of time step selection criteria in numerical simulations.** In the realm of engineering vibrations, the selection of appropriate time steps holds immense significance for the accuracy and stability of numerical simulations. This study meticulously examines the criteria involved in determining the optimal time interval for simulations, specifically focusing on the analysis of natural frequencies and mode shapes. By delving into these essential parameters, our aim is to establish a robust methodology for selecting time steps that can greatly enhance the integrity of simulation results.

The critical evaluation commences by computing the natural frequencies and mode shapes of the system through an eigenvalue decomposition of the structural stiffness matrix (K) and the mass matrix (M). The resulting eigenvectors (ϕ) and eigenvalues (ω_n) serve as foundational components for subsequent analyses.

$$[\phi, \omega_n] = \text{eig}(K, M). \tag{4}$$

Subsequently, we pinpoint the maximum natural frequency ($\omega_{\max}$), which serves as a crucial parameter for determining the maximum permissible time step. The calculation of the maximum natural frequency is conducted as follows:

$$\omega_{\max} = \sqrt{\max(\omega_n)}. \tag{5}$$

The frequency corresponding to the maximum natural frequency can be expressed as

$$f_{\max} = \frac{\omega_{\max}}{2\pi}. \tag{6}$$

The time step (Δt) is then defined through the relation:

$$\Delta t = \frac{1}{\alpha \cdot f_{\max}}. \tag{7}$$

Of particular importance is the identification of the maximum natural frequency ($\omega_{\max}$), which plays a crucial role in determining the maximum permissible time step. By calculating this key parameter, we can effectively establish an appropriate time step that ensures the stability and accuracy of the simulation results. The utilization of the Courant-Friedrichs-Lewy (CFL) condition, coupled with a safety factor $\alpha = 2$, further strengthens the selection process by considering the system's highest natural frequency.

Ultimately, the proposed methodology for time step selection, rooted in the estimation of natural frequencies and mode shapes, promises a stable and accurate numerical solution. By integrating a time scaling factor, the time step can be tailored to suit the specific requirements of the simulation, striking a balance between computational efficiency and result precision.

4. **Direct Integration Solution of the Equilibrium Equations in Dynamic Analysis.** Evaluating the dynamic response of a linear multi-degree-of-freedom (MDOF) structure optimally involves partitioning the response time history into short time increments. Throughout each increment, structural properties are assumed constant. Following each step, these properties update to align with current deformation conditions. Notably, this method is equally applicable to linear MDOF systems, where updating properties is unnecessary.

4.1. **Linear equations of motion in matrix form.** The matrix form of the linear equations of motion for the wheelchair-occupant system was derived using the parameters and variables in Figures 1 and 2 and Tables 1 and 2. The incremental form of the equation of motion for a linear MDOF system is given by

$$[M]\{\ddot{y}(t+\Delta t)\} + [C]\{\dot{y}(t+\Delta t)\} + [K]\{y(t+\Delta t)\} = \{F(t+\Delta t)\}. \tag{8}$$

The model with harmonic input excitation was analyzed using this approach, which yields the system's steady-state response. The equation of motion in matrix form is given by

$$[M] = \begin{bmatrix} m_{11} & m_{12} & \dots & m_{1j} \\ \vdots & \vdots & \ddots & \vdots \\ m_{i1} & m_{i2} & \dots & m_{ij} \end{bmatrix}, \quad [K] = \begin{bmatrix} k_{11} & k_{12} & \dots & k_{1j} \\ \vdots & \vdots & \ddots & \vdots \\ k_{i1} & k_{i2} & \dots & k_{ij} \end{bmatrix}, \quad [C] = \begin{bmatrix} c_{11} & c_{12} & \dots & c_{1j} \\ \vdots & \vdots & \ddots & \vdots \\ c_{i1} & c_{i2} & \dots & c_{ij} \end{bmatrix}, \tag{9}$$

where $[M] = [m_{ij}] \in R^{ij\times ij}$ represents mass matrix of time at $t+\Delta t$, [Kg]. $[K] = [k_{ij}] \in R^{ij\times ij}$ represents stiffness matrix of time at $t+\Delta t$, [N/m]. $[C] = [c_{ij}] \in R^{ij\times ij}$ represents damping matrix of time at $t+\Delta t$, [Ns/m]. $\{\ddot{y}(t+\Delta t)\} = \{\ddot{y}_{ij}(t_{n+1})\} \in R^{ij\times 1}$ represents acceleration vector of time at $t+\Delta t$, [m^2/s]. $\{\dot{y}(t+\Delta t)\} = \{\dot{y}_{ij}(t_{n+1})\} \in R^{ij\times 1}$ represents velocity vector of time at $t+\Delta t$, [m/s]. $\{y(t+\Delta t)\} = \{y_{ij}(t_{n+1})\} \in R^{ij\times 1}$ represents displacement vector of time at $t+\Delta t$, [m]. $\{F(t+\Delta t)\} = \{F_{ij}(t_{n+1})\} \in R^{ij\times 1}$ represents excitation force transpose of vector of time at $t+\Delta t$, [N/m^2]. They are equivalent to the assumption that the stiffness and damping force are linear within t and $t+\Delta t$ by using Piecewise linear approximation of structural system as Equation (8).

The equations of motion for a wheelchair-occupant system are derived, considering displacement, velocity and acceleration. The model combines mass, damping, stiffness and force harmonic excitation, reaching steady state infinitely. The mathematical model used to analyze the dynamics of the system shown in Figures 1 and 2 is based on previous studies [20, 34, 35, 33, 48].

4.2. **Numerical solution and method selection.** In this study, the Newmark method was selected for solving the equations of motion in analyzing seat transmissibility in wheelchairs due to its robustness and suitability for dynamic systems. This implicit time integration technique is particularly effective for handling the stiffness and mass matrices associated with multi-degree-of-freedom (MDOF) systems. Its capability to maintain numerical stability and control numerical damping across various frequencies makes it highly effective for vibration analysis.

Comparison with Other Numerical Methods: i) Runge-Kutta Method: The fourth-order Runge-Kutta methods are explicit methods praised for their accuracy in solving ordinary differential equations. However, they can be computationally intensive and less stable in stiff systems, requiring smaller time steps to ensure accuracy, rendering them less suitable for systems like the wheelchair-human body interaction where stiffness is significant. ii) Finite Element Method (FEM): FEM is a powerful tool for spatial discretization that, when coupled with time integration methods like the Newmark method, provides comprehensive insights into dynamic behaviors. However, FEM primarily addresses the spatial domain and must be paired with robust time integration techniques to effectively solve

dynamic problems. Thus, while FEM could be used for spatial analysis, the Newmark method's role in time integration is critical for accurately capturing dynamic responses.

Justification for Choosing the Newmark Method Numerical Stability: The implicit nature of the Newmark method ensures stability, which is essential for accurately simulating the dynamic response of stiff systems like the wheelchair-human body interaction.

Control of Numerical Damping: The Newmark method's parameters allow explicit control over numerical damping, facilitating fine-tuning of the model to accurately reflect real-world damping characteristics.

Compatibility with MDOF Systems: The method's suitability for MDOF systems ensures effective capture of coupled dynamic behaviors, vital for the wheelchair-human body system.

Robustness and Reliability: The Newmark method's established track record in structural dynamics and vibration analysis underscores its reliability, making it the optimal choice for this study.

Implications for Wheelchair Cushion Design: The results obtained using the Newmark method, validated by strong correlation with empirical data, demonstrate its efficacy in predicting transmissibility and informing wheelchair cushion design. This model provides a crucial tool for clinicians and engineers, enhancing rider comfort and minimizing the risk of vibration-related health issues.

4.3. **Newmark integration of linear structure.** Newmark [40, 43] proposed a single step-single solve procedure to calculate the displacement increment from the velocity integral:

$$y(t_{n+1}) = y(t_n + \Delta t) = y(t_n) + \int_{t_n}^{t_{n+1}} \dot{y}(\tau) d\tau, \tag{10}$$

where τ is a dummy variable of integration that represents any time point between t_n and t_{n+1}. By differentiating this equation with respect to time, the velocity at $t_{n+1} = t_n + \Delta t$ can be obtained as

$$\dot{y}(t_{n+1}) = \dot{y}(t_n) + \int_{t_n}^{t_{n+1}} \ddot{y}(\tau) d\tau. \tag{11}$$

Using integration by parts, the displacement equation (10) can be rewritten as

$$y(t_{n+1}) = y(t_n) - [(t_{n+1} - \tau)\dot{y}(\tau)]_{t_n}^{t_{n+1}} + \int_{t_n}^{t_{n+1}} (t_{n+1} - \tau)\ddot{y}(\tau) d\tau, \tag{12}$$

where the term $\int 1 d\tau = \tau - t_{n+1}$ is expressed relative to t_{n+1} and the term $[\ ]_n^{n+1}$ vanishes at the upper limit $\tau = t_{n+1}$. These relations (13) and (14) lead to the Newmark integrals, which are used to approximate the velocity and displacement at the next time step. The velocity at $t + \Delta t$ can be calculated as follows:

$$\dot{y}(t_{n+1}) = \dot{y}(t_n) + \int_{t_n}^{t_{n+1}} \ddot{y}(\tau) d\tau. \tag{13}$$

And the displacement change from time t to $t + \Delta t$ is obtained as

$$y(t_{n+1}) = y(t_n) + \Delta t \dot{y}(t_n) + \int_{t_n}^{t_{n+1}} (t_{n+1} - \tau)\ddot{y}(\tau) d\tau. \tag{14}$$

4.4. **Single-step expressions.** The integrals in the equations of motion were approximated as weighted mean values, following the method proposed by [40, 43]. This simplifies the numerical integration and reduces the computational cost. The approximation is given by

$$\int_{t_n}^{t_{n+1}} \ddot{y}(\tau)d\tau \simeq (1-\gamma)\Delta t\ddot{y}(t_n) + \gamma\Delta t\ddot{y}(t_{n+1}), \tag{15}$$

$$\int_{t_n}^{t_{n+1}} (t_{n+1}-\tau)\ddot{y}(\tau)d\tau \simeq \left(\frac{1}{2}-\beta\right)(\Delta t)^2\ddot{y}(t_n) + \beta(\Delta t)^2\ddot{y}(t_{n+1}), \tag{16}$$

where Δt is the time step and γ and β are the Newmark's method parameters that determine relative forward weights. The values of γ and β should satisfy $0 < \gamma < 1$ and $0 < \beta < \frac{1}{2}$ for stability and accuracy. Using these approximations, the velocity value at $\dot{y}(t_{n+1})$ and the acceleration value at $\ddot{y}(\hat{\tau})$ were obtained by solving Equations (15) and (16), respectively. These expressions are derived from the Newmark's method and the Duhamel's integral [40] and are important for calculating the dynamic response of the system under harmonic excitation. The expressions for $\dot{y}(t_{n+1})$ and $\ddot{y}(\hat{\tau})$ are given by

$$\dot{y}(t_{n+1}) = \dot{y}(t_n) + (1-\gamma)\Delta t\ddot{y}(t_n) + \gamma\Delta t\ddot{y}(t_{n+1}), \tag{17}$$

$$\ddot{y}(\hat{\tau}) = 2\beta\{\ddot{y}(t_{n+1})\} + (1-2\beta)\{\ddot{y}(t_n)\}, \quad t_n \le \hat{\tau} \le t_{n+1} \tag{18}$$

where $\hat{\tau}$ is an intermediate time point between t_n and t_{n+1}. The equations and methods used in this analysis were based on the works of [40].

4.4.1. *Numerical implementation of Newmark algorithms.* The prediction and correction steps of the Newmark algorithms for solving the equations of motion of the 13-DOF model are described in this subsection. The mass, stiffness and damping matrices are denoted by $[M]$, $[K]$ and $[C]$, respectively and have dimensions of 13×13. The displacement, velocity and acceleration response vectors are denoted by $y(t)$, $\dot{y}(t)$ and $\ddot{y}(t)$, respectively and have dimensions of 13×1. The excitation frequency is denoted by ω. Equations of Motion and System Parameters. This subsection explains the terms and parameters of the EOMs derived from Equations (1)∼(18). The mass matrix has only diagonal elements that represent the mass-related forces. The EOMs define the elements of the mass matrix. The excitation stiffness ($[K_0]$) and damping ($[C_0]$) matrices have dimensions of 13×1 and affect the 10th, 11th, 12th and 13th rows of the EOMs. These rows correspond to the sinusoidal forces given by Equations (34)∼(36), which represent the external excitation forces. The EOMs in matrix form provide a concise representation of the system dynamics, which include mass, stiffness, damping and external forces. These equations enable the analysis of the wheelchair-occupant system and its response under various conditions [45].

4.4.2. *Theoretical framework: Displacement approximation by Taylor series expansion.* Expanding the displacement $\{y(t_{n+1})\}$ in a second Taylor series provides

$$\{y(t_{n+1})\} = \{y(t_n)\} + \Delta t\{\dot{y}(t_n)\} + \frac{(\Delta t)^2}{2}\{\ddot{y}(\hat{\tau})\}, \quad t_n \le \hat{\tau} \le t_{n+1}. \tag{19}$$

4.4.3. *Formulation and solution of Newmark time integration.* The displacement formula as a function of the new acceleration is derived by substituting Equation (18) into Equation (19) as shown in Equation (20):

$$\{y(t_{n+1})\} = \{y(t_n)\} + \Delta t\{\dot{y}(t_n)\} + \frac{(\Delta t)^2}{2}(2\beta\{\ddot{y}(t_{n+1})\} + (1-2\beta)\{\ddot{y}(t_n)\}). \tag{20}$$

The displacement formula is rearranged as a function of the new acceleration and solved for $\{\ddot{y}(t_{n+1})\}$, obtaining

$$\{\ddot{y}(t_{n+1})\} = \frac{1}{\beta(\Delta t)^2}(\{y(t_{n+1})\} - \{y(t_n)\} - \Delta t\{\dot{y}(t_n)\}) - \frac{1-2\beta}{2\beta}\{\ddot{y}(t_n)\}. \tag{21}$$

This expression is substituted into the velocity formula:

$$\{\dot{y}(t_{n+1})\} = \frac{\gamma}{\beta\Delta t}(\{y(t_{n+1})\} - \{y(t_n)\} - \Delta t\{\dot{y}(t_n)\}) - \gamma\Delta t\frac{1-2\beta}{2\beta}\{\ddot{y}(t_n)\} + \Delta t(1-\gamma)\{\ddot{y}(t_n)\}. \quad (22)$$

Equation (22) is rearranged and obtained:

$$\{\dot{y}(t_{n+1})\} = \frac{\gamma}{\beta\Delta t}(\{y(t_{n+1})\} - \{y(t_n)\}) + \left(1-\frac{\gamma}{\beta}\right)\{\dot{y}(t_n)\} + \Delta t\left(1-\frac{\gamma}{2\beta}\right)\{\ddot{y}(t_n)\}. \quad (23)$$

4.4.4. *Solution of EOMs by implicit time integration.* The EOMs at time $t+\Delta t$ are solved by finding the displacement, velocity and acceleration from Equations (20) to (23). They are substituted into Equation (8), obtaining

$$[M]\left(\frac{1}{\beta(\Delta t)^2}(\{y(t_{n+1})\} - \{y(t_n)\} - \Delta t\{\dot{y}(t_n)\}) - \frac{1-2\beta}{2\beta}\{\ddot{y}(t_n)\}\right) + [C]\left(\frac{\gamma}{\beta\Delta t}(\{y(t_{n+1})\} - \{y(t_n)\}) + \left(1-\frac{\gamma}{\beta}\right)\{\dot{y}(t_n)\} + \Delta t\left(1-\frac{\gamma}{2\beta}\right)\{\ddot{y}(t_n)\}\right) + [K]\{y(t_{n+1})\} = \{F(t_{n+1})\}. \quad (24)$$

Equation (24) is solved and the displacement values for each DOF of the body segments and wheelchair components are obtained as Equation (25).

$$\{y(t_{n+1})\} = \left[[M]\frac{1}{\beta(\Delta t)^2} + [C]\frac{\gamma}{\beta\Delta t} + [K]\right]^{-1}\{F(t_{n+1})\} + [M]\left(\frac{1}{\beta(\Delta t)^2}(\{y(t_n)\} + \Delta t\{\dot{y}(t_n)\}) + \frac{1-2\beta}{2\beta}\{\ddot{y}(t_n)\}\right) + [C]\left(\frac{\gamma}{\beta\Delta t}\{y(t_n)\} - \left(1-\frac{\gamma}{\beta}\right)\{\dot{y}(t_n)\} - \Delta t\left(1-\frac{\gamma}{2\beta}\right)\{\ddot{y}(t_n)\}\right). \quad (25)$$

$\{y(t_{n+1})\}$ from Equation (25) is substituted into Equation (23) and the velocity values for each DOF of the body segments and wheelchair components in the MODF system are obtained as Equation (26).

$$\{\dot{y}(t_{n+1})\} = \frac{\gamma}{\beta\Delta t}\left(\left[[M]\frac{1}{\beta(\Delta t)^2} + [C]\frac{\gamma}{\beta\Delta t} + [K]\right]^{-1}\{F(t_{n+1})\} + [M]\left(\frac{1}{\beta(\Delta t)^2}(\{y(t_n)\} + \Delta t\{\dot{y}(t_n)\}) + \frac{1-2\beta}{2\beta}\{\ddot{y}(t_n)\}\right) + [C]\left(\frac{\gamma}{\beta\Delta t}\{y(t_n)\} - \left(1-\frac{\gamma}{\beta}\right)\{\dot{y}(t_n)\} - \Delta t\left(1-\frac{\gamma}{2\beta}\right)\{\ddot{y}(t_n)\}\right) - \{y(t_n)\}\right) - \Delta t\{\dot{y}(t_n)\} - \gamma\Delta t\frac{1-2\beta}{2\beta}\{\ddot{y}(t_n)\} + \Delta t(1-\gamma)\{\ddot{y}(t_n)\}. \quad (26)$$

$\{y(t_{n+1})\}$ from Equation (25) is substituted into Equation (21) and the acceleration values for each DOF of the body segments and wheelchair components in the MODF system are obtained as Equation (27).

$$\{\ddot{y}(t_{n+1})\} = \frac{1}{\beta(\Delta t)^2}\left(\left[[M]\frac{1}{\beta(\Delta t)^2} + [C]\frac{\gamma}{\beta\Delta t} + [K]\right]^{-1}\{F(t_{n+1})\} + [M]\left(\frac{1}{\beta(\Delta t)^2}(\{y(t_n)\} + \Delta t\{\dot{y}(t_n)\}) + \frac{1-2\beta}{2\beta}\{\ddot{y}(t_n)\}\right)\right.$$

$$+[C]\left(\frac{\gamma}{\beta\Delta t}\{y(t_n)\}-\left(1-\frac{\gamma}{\beta}\right)\{\dot{y}(t_n)\}-\Delta t\left(1-\frac{\gamma}{2\beta}\right)\{\ddot{y}(t_n)\}\right)$$
$$-\{y(t_n)\}-\Delta t\{\dot{y}(t_n)\}\Bigg)-\frac{1-2\beta}{2\beta}\{\ddot{y}(t_n)\}. \tag{27}$$

4.4.5. *Optimal parameters for vibration analysis.* The accuracy and stability of the acceleration approximation are influenced by the parameters γ and β, which act as weights. Second-order accuracy is ensured by the parameter $\gamma = \frac{1}{2}$ and $\beta = \frac{1}{6}$ while the choice corresponds to the linear acceleration method, which assumes a linear variation of acceleration during the time step. These choices balance stability and accuracy for the Newmark algorithms. The Newmark's method equations are transformed from the time domain to the frequency domain by starting with the given equations. A second-order ordinary differential equation governing the motion of a linear system is addressed by the Newmark-beta method. The application of the Fourier transform to both sides is required for the transformation of this equation from the time domain to the frequency domain. The Fourier transform of a function $F(t)$ is denoted by $\mathcal{F}[F(t)]$ or $\hat{F}(\omega)$, where ω is the angular frequency.

4.5. **The Fourier transform.** The Fourier transform [49] is a mathematical operation that changes a signal from time domain to frequency domain. The equations of the Newmark's method are transformed from the time domain to the frequency domain by starting with the given equations. A second-order ordinary differential equation governing the motion of a linear system is addressed by the Newmark-beta method. Both sides of this equation are subjected to the Fourier transform for the transformation from the time domain to the frequency domain. The Fourier transform of a function $F(t)$ is denoted by $\mathcal{F}[F(t)]$ or $\hat{F}(\omega)$, where ω is the angular frequency. The Fourier transform is defined as follows:

$$\mathcal{F}[F(t)] = \hat{F}(\omega) = \int_{-\infty}^{\infty} F(t)e^{j\omega t}dt, \tag{28}$$

where j is the imaginary unit. $\mathcal{F}$ is the Fourier transform. Several properties of the Fourier transform, detailed in Equation (28), is valuable for transforming the Newmark-beta equation. It is noteworthy that the Fourier transform of the external force vector $F(t)$ depends on the nature of the force and the input frequency range. For example, if the force is harmonic, the Fourier transform will exhibit a peak at the frequency of the force.

4.5.1. *Exponential function vectors of the response.* The derivatives of the equation describing the response to vibrations are given by

$$\begin{cases} \mathcal{F}\{y(t)\} = e^{j\omega t}\mathcal{F}\{y(t)\} = e^{j\omega t}\{\hat{y}(\omega)\} \\ \mathcal{F}\{\dot{y}(t)\} = j\omega\mathcal{F}\{y(t)\} = j\omega e^{j\omega t}\{\hat{y}(\omega)\} \\ \mathcal{F}\{\ddot{y}(t)\} = -\omega^2\mathcal{F}\{y(t)\} = -\omega^2 e^{j\omega t}\{\hat{y}(\omega)\} \end{cases}, \tag{29}$$

where $\mathcal{F}$ denotes the Fourier Transform, ω is the frequency and j is the imaginary unit. Let $\hat{y}(\omega)$ represent the Fourier transform of $y(t)$.

4.5.2. *Exponential function vectors of excitation.* The derivatives of the equation describing excitation from the base state are expressed as follows:

$$\begin{cases} \mathcal{F}\{F(t)\} = \left\{\hat{F}(\omega)\right\}e^{j\omega t} \\ \mathcal{F}\{\dot{y_0}(t)\} = j\omega\{\hat{y_0}(\omega)\}e^{j\omega t} \end{cases}, \tag{30}$$

where $\{\dot{y_0}(t)\}$ represents the magnitude of the input displacement excitation vector. To transition Newmark's method equations into the frequency domain, Fourier transforms are employed. $\hat{F}(\omega)$ denotes the Fourier transform of $F(t)$ and $\omega = 2\pi f$ represents the angular frequency.

4.5.3. *Frequency-domain equations of Newmark's method.* The system of equations for Newmark's method in the frequency domain can be solved by expressing them in a compact form and finding the unknowns $\hat{y}(\omega)$, $\hat{\dot{y}}(\omega)$ and $\hat{\ddot{y}}(\omega)$. These solutions are complex and may require numerical methods, depending on the matrices and forces involved. The specific steps vary according to the problem details.

The Fourier transform, $\hat{F}(\omega)$, gives the sinusoidal signal amplitude at each frequency, where $\{F(t)\}$ is the input force excitation vector magnitude and $e^{j\omega t}$ is a complex exponential term. Substituting these expressions into the original equations and replacing $F(t)$, $y(t)$, $\dot{y}(t)$, $\ddot{y}(t)$ of Equations (28)∼(30) in Equations (25)∼(27), we obtain the frequency domain equations for the MODF system:

$$\begin{aligned}
\{\hat{y}(\omega)\} = {} & \frac{1}{[M]\frac{1}{\beta(\Delta t)^2} + [C]\frac{\gamma}{\beta\Delta t} + [K]} \left\{\hat{F}(\omega)\right\} \\
& + \left[\frac{[M]}{\beta(\Delta t)^2} + \frac{[C]\gamma}{\beta\Delta t} + [K]\right] \left(\frac{1}{\beta(\Delta t)^2}\{\hat{y}(\omega)\} + \Delta t \cdot j\omega\{\hat{y}(\omega)\}\right) \\
& + \left[[C]\frac{\gamma}{\beta\Delta t} - \left(1 - \frac{\gamma}{\beta}\right) \cdot j\omega - \Delta t \left(1 - \frac{\gamma}{2\beta}\right) \cdot (j\omega)^2\right] \frac{\gamma}{\beta\Delta t}\{\hat{y}(\omega)\}, \quad (31) \\
\left\{\hat{\dot{y}}(\omega)\right\} = {} & \frac{\gamma}{\beta\Delta t} \left(\frac{1}{[M]\frac{1}{\beta(\Delta t)^2} + [C]\frac{\gamma}{\beta\Delta t} + [K]} \left\{\hat{F}(\omega)\right\}\right) \\
& + \left[\frac{[M]}{\beta(\Delta t)^2} + \frac{[C]\gamma}{\beta\Delta t} + [K]\right] \left(\frac{1}{\beta(\Delta t)^2}\{\hat{y}(\omega)\} + \Delta t \cdot j\omega\{\hat{y}(\omega)\}\right) \\
& + \left[[C]\frac{\gamma}{\beta\Delta t} - \left(1 - \frac{\gamma}{\beta}\right) \cdot j\omega - \Delta t \left(1 - \frac{\gamma}{2\beta}\right) \cdot (j\omega)^2\right] \frac{\gamma}{\beta\Delta t}\{\hat{y}(\omega)\} \\
& - \Delta t \cdot \{\hat{y}(\omega)\} - \Delta t \cdot j\omega\{\hat{y}(\omega)\} - \gamma\Delta t \frac{1 - 2\beta}{2\beta} \cdot (j\omega)^2\{\hat{y}(\omega)\} \\
& + \Delta t(1 - \gamma) \cdot (j\omega)^2\{\hat{y}(\omega)\}, \quad (32) \\
\left\{\hat{\ddot{y}}(\omega)\right\} = {} & \frac{1}{\beta(\Delta t)^2} \left(\frac{1}{[M]\frac{1}{\beta(\Delta t)^2} + [C]\frac{\gamma}{\beta\Delta t} + [K]} \left\{\hat{F}(\omega)\right\}\right) \\
& + \left[\frac{[M]}{\beta(\Delta t)^2} + \frac{[C]\gamma}{\beta\Delta t} + [K]\right] \left(\frac{1}{\beta(\Delta t)^2}\{\hat{y}(\omega)\} + \Delta t \cdot j\omega\,\{\hat{y}(\omega)\}\right) \\
& + \left[[C]\frac{\gamma}{\beta\Delta t} - \left(1 - \frac{\gamma}{\beta}\right) \cdot j\omega - \Delta t \left(1 - \frac{\gamma}{2\beta}\right) \cdot (j\omega)^2\right] \frac{\gamma}{\beta\Delta t}\{\hat{y}(\omega)\} \\
& - \Delta t \cdot \{\hat{y}(\omega)\} - \Delta t \cdot j\omega\{\hat{y}(\omega)\} - \frac{1 - 2\beta}{2\beta} \cdot (j\omega)^2\{\hat{y}(\omega)\}. \quad (33)
\end{aligned}$$

The simulation of the 13-linear differential equations produces the frequency domain responses of displacement, velocity and acceleration vectors, $\{\hat{y}(\omega)\}$, $\left\{\hat{\dot{y}}(\omega)\right\}$ and $\left\{\hat{\ddot{y}}(\omega)\right\}$, to the steady-state sinusoidal inputs at various vibration frequencies. The amplitude ratios are obtained by dividing the body parts and wheelchair responses by the input vibration amplitude.

5. **Numerical Example.** These equations of motion describe the dynamic behavior of the 13-DOF wheelchair-occupant model. The mass, stiffness and damping characteristics of the model are expressed as 13 by 13 matrices denoted by $[M]$, $[K]$ and $[C]$. Each matrix, upon being multiplied with $\{\ddot{y}(t)\}$, $\{\dot{y}(t)\}$ and $\{y(t)\}$ yields acceleration, velocity and displacement vectors of the system – all of which being dependent on the characteristics of force. $\{F\}$ is the harmonic excitation force vectors; ω represents the excitation frequency; while $[K_0]$ and $[C_0]$, the stiffness and damping matrices at excitation $\{y_0(t)\}$ and $\{\dot{y}_0(t)\}$, the resulting displacement and velocity vectors upon excitation and response of the wheelchair-occupant system under various conditions and inputs. Relationships of these variables can be expressed in matrix and vector forms as shown in Equations (34) and (35):

$$[M]\{\ddot{y}(t)\} + [C]\{\dot{y}(t)\} + [K]\{y(t)\} = \{F(t)\}, \tag{34}$$

$$\{F(t)\} = [K_0]\{y_0(t)\} + [C_0]\{\dot{y}_0(t)\}. \tag{35}$$

5.1. **Derivation of EOMs in matrix form.** The governing EOM for each mass consists of its inertia term and forces exerted on it by the stiffnesses and dampers due to the relative motion of the connected masses. In an EOM, each of the variables – including $[M] = [m_{ij}]$, $[K] = [k_{ij}]$, $[C] = [c_{ij}]$, $\{y(t)\} = \{y_{i1}\}$, $\{\dot{y}(t)\} = \{\dot{y}_{i1}\}$ and $\{\ddot{y}(t)\} = \{\ddot{y}_{i1}\}$ – is subscripted with a number from 1 to 13 that represents an assigned component (i.e., $(i = 1, 2, \ldots, 13)$ whereby 1 to 7 denote the body parts; and 8 to 13 being the wheelchair components). In addition, $\{y_0(t)\}$ and $\{\dot{y}_0(t)\}$ respectively refer to the input displacement and velocity vector of the tire contact points to the floor. As the floor surface will cause the tires to compress, $y_0(t)$ and $\dot{y}_0(t)$ are, respectively, the amplitude of input displacement excitation and circular frequency of this displacement applied at the tire contact points.

The above eleven linear differential equations are solved by computer simulation to yield $\{\ddot{y}_{i1}\}$, $\{\dot{y}_{i1}\}$ and $\{y_{i1}\}$ $(i = 1, 2, \ldots, 13)$, which are the corresponding accelerations, velocities and displacements occurring as responses to vibration waves at different frequencies. By dividing the amplitude response of each body part by its corresponding input amplitude, the amplitude ratios of that body part are computed. Similarly, the amplitude ratios of the wheelchair parts can be likewise determined. The transmissibility of different seat cushions is then determined in relation to the responses of the body parts in the 0.5 to 20 [Hz] frequency range. The parameters of the body parts and wheelchair, which give the maximum vibration responses of the body parts, are listed in Tables 1 and 2.

$$\begin{bmatrix} m_1 & 0 & 0 & 0 & 0 & 0 & 0 & 0 & 0 & 0 & 0 & 0 & 0 \\ 0 & m_2 & 0 & 0 & 0 & 0 & 0 & 0 & 0 & 0 & 0 & 0 & 0 \\ 0 & 0 & m_3 & 0 & 0 & 0 & 0 & 0 & 0 & 0 & 0 & 0 & 0 \\ 0 & 0 & 0 & m_4 & 0 & 0 & 0 & 0 & 0 & 0 & 0 & 0 & 0 \\ 0 & 0 & 0 & 0 & m_5 & 0 & 0 & 0 & 0 & 0 & 0 & 0 & 0 \\ 0 & 0 & 0 & 0 & 0 & m_6 & 0 & 0 & 0 & 0 & 0 & 0 & 0 \\ 0 & 0 & 0 & 0 & 0 & 0 & m_7 & 0 & 0 & 0 & 0 & 0 & 0 \\ 0 & 0 & 0 & 0 & 0 & 0 & 0 & m_8 & 0 & 0 & 0 & 0 & 0 \\ 0 & 0 & 0 & 0 & 0 & 0 & 0 & 0 & m_9 & 0 & 0 & 0 & 0 \\ 0 & 0 & 0 & 0 & 0 & 0 & 0 & 0 & 0 & m_{10} & 0 & 0 & 0 \\ 0 & 0 & 0 & 0 & 0 & 0 & 0 & 0 & 0 & 0 & m_{11} & 0 & 0 \\ 0 & 0 & 0 & 0 & 0 & 0 & 0 & 0 & 0 & 0 & 0 & m_{12} & 0 \\ 0 & 0 & 0 & 0 & 0 & 0 & 0 & 0 & 0 & 0 & 0 & 0 & m_{13} \end{bmatrix} \begin{Bmatrix} \ddot{y}_1 \\ \ddot{y}_2 \\ \ddot{y}_3 \\ \ddot{y}_4 \\ \ddot{y}_5 \\ \ddot{y}_6 \\ \ddot{y}_7 \\ \ddot{y}_8 \\ \ddot{y}_9 \\ \ddot{y}_{10} \\ \ddot{y}_{11} \\ \ddot{y}_{12} \\ \ddot{y}_{13} \end{Bmatrix}$$

$$
+\begin{bmatrix}
c_1 & -c_1 & 0 & 0 & 0 & 0 & 0 & 0 & 0 & 0 & 0 & 0 & 0 \\
-c_1 & A_{01} & -c_{32} & 0 & 0 & -c_2 & 0 & 0 & 0 & 0 & 0 & 0 & 0 \\
0 & -c_{32} & A_{02} & -c_3 & 0 & 0 & 0 & 0 & 0 & 0 & 0 & 0 & 0 \\
0 & 0 & -c_3 & A_{03} & -c_4 & 0 & 0 & 0 & 0 & 0 & 0 & 0 & 0 \\
0 & 0 & 0 & -c_4 & A_{04} & -c_5 & 0 & 0 & 0 & 0 & 0 & 0 & 0 \\
0 & 0 & 0 & 0 & -c_5 & A_{05} & -c_6 & 0 & 0 & 0 & 0 & 0 & 0 \\
0 & -c_2 & 0 & 0 & 0 & -c_6 & A_{06} & -c_7 & 0 & 0 & 0 & 0 & 0 \\
0 & 0 & 0 & 0 & 0 & 0 & -c_7 & A_{07} & -c_8 & 0 & 0 & 0 & 0 \\
0 & 0 & 0 & 0 & 0 & 0 & 0 & -c_8 & A_{08} & -c_{9f} & -c_{9f} & -c_{9r} & -c_{9r} \\
0 & 0 & 0 & 0 & 0 & 0 & 0 & 0 & -c_{9f} & A_{09} & 0 & 0 & 0 \\
0 & 0 & 0 & 0 & 0 & 0 & 0 & 0 & -c_{9f} & 0 & A_{10} & 0 & 0 \\
0 & 0 & 0 & 0 & 0 & 0 & 0 & 0 & -c_{9r} & 0 & 0 & A_{11} & 0 \\
0 & 0 & 0 & 0 & 0 & 0 & 0 & 0 & -c_{9r} & 0 & 0 & 0 & A_{12}
\end{bmatrix}
\begin{Bmatrix}
\dot{y}_1 \\ \dot{y}_2 \\ \dot{y}_3 \\ \dot{y}_4 \\ \dot{y}_5 \\ \dot{y}_6 \\ \dot{y}_7 \\ \dot{y}_8 \\ \dot{y}_9 \\ \dot{y}_{10} \\ \dot{y}_{11} \\ \dot{y}_{12} \\ \dot{y}_{13}
\end{Bmatrix}
$$

$$
+\begin{bmatrix}
k_1 & -k_1 & 0 & 0 & 0 & 0 & 0 & 0 & 0 & 0 & 0 & 0 & 0 \\
-k_1 & B_{01} & -k_{32} & 0 & 0 & -k_2 & 0 & 0 & 0 & 0 & 0 & 0 & 0 \\
0 & -k_{32} & B_{02} & -k_3 & 0 & 0 & 0 & 0 & 0 & 0 & 0 & 0 & 0 \\
0 & 0 & -k_3 & B_{03} & -k_4 & 0 & 0 & 0 & 0 & 0 & 0 & 0 & 0 \\
0 & 0 & 0 & -k_4 & B_{04} & -k_5 & 0 & 0 & 0 & 0 & 0 & 0 & 0 \\
0 & 0 & 0 & 0 & -k_5 & B_{05} & -k_6 & 0 & 0 & 0 & 0 & 0 & 0 \\
0 & -k_2 & 0 & 0 & 0 & -k_6 & B_{06} & -k_7 & 0 & 0 & 0 & 0 & 0 \\
0 & 0 & 0 & 0 & 0 & 0 & -k_7 & B_{07} & -k_8 & 0 & 0 & 0 & 0 \\
0 & 0 & 0 & 0 & 0 & 0 & 0 & -k_8 & B_{08} & -k_{9f} & -k_{9f} & -k_{9r} & -k_{9r} \\
0 & 0 & 0 & 0 & 0 & 0 & 0 & 0 & -k_{9f} & B_{09} & 0 & 0 & 0 \\
0 & 0 & 0 & 0 & 0 & 0 & 0 & 0 & -k_{9f} & 0 & B_{10} & 0 & 0 \\
0 & 0 & 0 & 0 & 0 & 0 & 0 & 0 & -k_{9r} & 0 & 0 & B_{11} & 0 \\
0 & 0 & 0 & 0 & 0 & 0 & 0 & 0 & -k_{9r} & 0 & 0 & 0 & B_{12}
\end{bmatrix}
\begin{Bmatrix}
y_1 \\ y_2 \\ y_3 \\ y_4 \\ y_5 \\ y_6 \\ y_7 \\ y_8 \\ y_9 \\ y_{10} \\ y_{11} \\ y_{12} \\ y_{13}
\end{Bmatrix}
$$

$$
= \left\{ \begin{array}{cccccccccccc} 0 & 0 & 0 & 0 & 0 & 0 & 0 & 0 & 0 & k_{10}y_{10}\sin\omega t & k_{11}y_{11}\sin\omega t & k_{12}y_{12}\sin\omega t & k_{13}y_{13}\sin\omega t \end{array} \right\}^t
$$

$$
+ \left\{ \begin{array}{cccccccccccc} 0 & 0 & 0 & 0 & 0 & 0 & 0 & 0 & 0 & c_{10}\dot{y}_{10}\sin\omega t & c_{11}\dot{y}_{11}\sin\omega t & c_{12}\dot{y}_{12}\sin\omega t & c_{13}\dot{y}_{13}\sin\omega t \end{array} \right\}^t . \quad (36)
$$

Here

$$A_{01} = c_1 + c_2 + c_{32}, \quad (37)$$

$$A_{02} = c_{32} + c_3, \quad (38)$$

$$A_{03} = c_3 + c_4, \quad (39)$$

$$A_{04} = c_4 + c_5, \quad (40)$$

$$A_{05} = c_5 + c_6, \quad (41)$$

$$A_{06} = c_6 + c_7 + c_2, \quad (42)$$

$$A_{07} = c_7 + c_8, \quad (43)$$

$$A_{08} = c_8 + 2(c_{9f}) + 2(c_{9r}), \quad (44)$$

$$A_{09} = c_{9f} + c_{10}, \quad (45)$$

$$A_{10} = c_{9f} + c_{11}, \quad (46)$$

$$A_{11} = c_{12} + c_{9r}, \quad (47)$$

and

$$A_{12} = c_{13} + c_{9r}. \tag{48}$$

A_{01} to A_{12} represent variables in the positions of $[C]$ caused by the sum of the damping constant (c_i) as shown in Equations (37) to (48).

$$B_{01} = k_1 + k_2 + k_{32}, \tag{49}$$
$$B_{02} = k_{32} + k_3, \tag{50}$$
$$B_{03} = k_3 + k_4, \tag{51}$$
$$B_{04} = k_4 + k_5, \tag{52}$$
$$B_{05} = k_5 + k_6, \tag{53}$$
$$B_{06} = k_6 + k_7 + k_2, \tag{54}$$
$$B_{07} = k_7 + k_8, \tag{55}$$
$$B_{08} = k_8 + 2(k_{9f}) + 2(k_{9r}), \tag{56}$$
$$B_{09} = k_{9f} + k_{10}, \tag{57}$$
$$B_{10} = k_{9f} + k_{11}, \tag{58}$$
$$B_{11} = k_{12} + k_{9r}, \tag{59}$$

and

$$B_{12} = k_{13} + k_{9r}. \tag{60}$$

B_{01} to B_{12} represent variables in the positions of $[K]$ caused by the sum of the damping constant (k_i) as shown in Equations (49) to (60). The ensuing section presents a comprehensive analysis of the obtained results across different frequency ranges (0.5 to 20 [Hz]) for the specified sinusoidal input.

The elements of these matrices are obtained from the EOMs. With the mass matrix, $[M] \in R^{13\times13}$, its elements are zero except those on its diagonal, $\{y(t)\}$, $\{\dot{y}(t)\}$ and $\{\ddot{y}(t)\}$ represent the displacement (y_{i1}), velocity ($\dot{y}_{i1}$) and acceleration ($\ddot{y}_{i1}$) vector of response, respectively and $\{F\}$ is a 13×1 force matrix whose elements are zero except those on the 10th to 13th rows which represent the sinusoidal forces given in steady state vibration. $[K_0] \in R^{1\times13}$ represents the stiffness matrix of the excitation and $\{y_0(t)\}$ and $\{\dot{y}_0(t)\}$ represent displacement and velocity vectors of excitation and written as (36).

5.2. **Exponential function vectors of MDOF.**

5.2.1. *Input force excitation vectors on the wheelchair.* The input force excitation vectors on the wheelchair are expressed by

$$\text{i) The right front wheel: } F_{10}(t_{n+1}) = (c_{10}\dot{y}_{10} + k_{10}y_{10})\sin(\omega t_{n+1}), \tag{61}$$
$$\text{ii) The left front wheel: } F_{11}(t_{n+1}) = (c_{11}\dot{y}_{11} + k_{11}y_{11})\sin(\omega t_{n+1}), \tag{62}$$
$$\text{iii) The right rear wheel: } F_{12}(t_{n+1}) = (c_{12}\dot{y}_{12} + k_{12}y_{12})\sin(\omega t_{n+1}), \tag{63}$$
$$\text{iv) The left rear wheel: } F_{13}(t_{n+1}) = (c_{13}\dot{y}_{13} + k_{13}y_{13})\sin(\omega t_{n+1}). \tag{64}$$

5.2.2. *The force vector of excitation in the time domain.* The force vector of excitation in the time domain is then given by

$$\{F(t_{n+1})\} = F_{10}(t_{n+1}) + F_{11}(t_{n+1}) + F_{12}(t_{n+1}) + F_{13}(t_{n+1}), \tag{65}$$

where y_{10}, y_{11}, y_{12} and y_{13} denote the road surface amplitudes, approximated as sinusoidal shapes, corresponding to wheelchair motion with different displacements for each wheel – 5, 8, 10 and 15 [mm], respectively. ω is the angular frequency, defined as $\omega = 2\pi f$, where f is the frequency in the range of 0.5 to 20 [Hz]. The damping coefficients for the front

wheels are $c_{10} = c_{11}$ and for the rear wheels, $c_{12} = c_{13}$. Similarly, the stiffness values for the front wheels are $k_{10} = k_{11}$ and for the rear wheels, $k_{12} = k_{13}$. The variable t represents the time period. For each of these parameters, frequency responses and displacement values have been computed. Figures 1 and 2 illustrate the frequency responses, including transmissibility and acceleration, for different segments of the human body experiencing vertical vibrations. The frequencies range from 0.5∼20 [Hz] and the terrain amplitudes are y_{10}, y_{11}, y_{12} and y_{13}, corresponding to 5, 8, 10 and 15 [mm], respectively, during wheelchair motion.

5.2.3. *Frequency-domain transformation of the Newmark's method equations.* The Fourier transform can reveal the spectral characteristics and resonant frequencies of the system. Let $\hat{y}(\omega)$ denote the Fourier transform of $y(t)$, $\hat{F}(\omega)$ the Fourier transform of $F(t)$ and $\hat{F}_{10}(j\omega)$, $\hat{F}_{11}(j\omega)$, $\hat{F}_{12}(j\omega)$, $\hat{F}_{13}(j\omega)$ and $\hat{F}(\omega)$ represent the Fourier transforms of $\{F_{10}(t_{n+1})\}$, $\{F_{11}(t_{n+1})\}$, $\{F_{12}(t_{n+1})\}$, $\{F_{13}(t_{n+1})\}$ and $\{F(t_{n+1})\}$, respectively. The transformation and method used in this analysis were based on the works of [49, 50].

$$\text{i) The right front wheel: } \left\{\hat{F}_{10}(j\omega)\right\} = (c_{10}\hat{y}_{10}j\omega + k_{10}\hat{y}_{10})e^{j\omega(t_{n+1})}, \tag{66}$$

$$\text{ii) The left front wheel: } \left\{\hat{F}_{11}(j\omega)\right\} = (c_{11}\hat{y}_{11}j\omega + k_{11}\hat{y}_{11})e^{j\omega(t_{n+1})}, \tag{67}$$

$$\text{iii) The right rear wheel: } \left\{\hat{F}_{12}(j\omega)\right\} = (c_{12}\hat{y}_{12}j\omega + k_{12}\hat{y}_{12})e^{j\omega(t_{n+1})}, \tag{68}$$

$$\text{iv) The left rear wheel: } \left\{\hat{F}_{13}(j\omega)\right\} = (c_{13}\hat{y}_{13}j\omega + k_{13}\hat{y}_{13})e^{j\omega(t_{n+1})}. \tag{69}$$

In the frequency domain, each term transforms into its counterpart. The excitation force vector becomes

$$\left\{\hat{F}(j\omega)\right\} = \left\{\hat{F}_{10}(j\omega)\right\} + \left\{\hat{F}_{11}(j\omega)\right\} + \left\{\hat{F}_{12}(j\omega)\right\} + \left\{\hat{F}_{13}(j\omega)\right\}. \tag{70}$$

The displacement vectors of input excitation $\left\{\hat{\ddot{y}}_0(j\omega)\right\}$ are then given by

$$\{\hat{y}_0(j\omega)\} = \frac{\left\{\hat{F}(j\omega)\right\}}{(c_{10} + c_{11} + c_{12} + c_{13})j\omega + (k_{10} + k_{11} + k_{12} + k_{13})}. \tag{71}$$

5.3. **Frequency-domain solution of the MDOF system of EOMs.** The equations of motion (EOMs) of the multi-degree-of-freedom (MDOF) system were solved using the frequency-domain (FD) method, a robust numerical technique for linear and stationary problems. The primary focus was on the steady-state response under various input excitations [50]. The Newmark method, an FD method that approximates displacement, velocity and acceleration at each frequency step, was employed to transform the second-order differential EOMs from the time domain to the frequency domain. The Newmark method incorporates two parameters, γ and β, which govern both accuracy and stability. Validation of the model results was achieved by comparison with experimental data from previous studies, which served as reference benchmarks. These experimental data were derived from measurements of whole-body vibration of wheelchair occupants on various road surfaces and seat cushions. The metrics of transmissibility and goodness-of-fit (GOF) were utilized to evaluate the prediction accuracy for each model configuration.

5.3.1. *Transmissibility.* Transmissibility (T), also known as the force and displacement ratio, is defined as the ratio of the response magnitude of a particular mass segment to

the input excitation magnitude. Transmissibility is quantified as follows:

$$T = \frac{\left|\hat{F}_k(j\omega)\right|}{\left|\hat{F}_0(j\omega)\right|} = \frac{|\hat{y}_k(j\omega)|}{|\hat{y}_0(j\omega)|}, \quad k = 1, 2, \ldots, 13, \tag{72}$$

where $\left|\hat{F}_k(j\omega)\right|$ and $|\hat{y}_k(j\omega)|$ represent the magnitudes of the force and displacement response from the occupant's body part and the wheelchair part (m_k) of the target mass segment k in the frequency domain. Similarly, $\left|\hat{F}_0(j\omega)\right|$ and $|\hat{y}_0(j\omega)|$ represent the magnitudes of the input excitation on the wheelchair.

5.3.2. *Goodness-of-fit (ϵ).* Goodness-of-fit is a statistical technique employed to measure and evaluate the prediction accuracy of each model setup by comparing simulation results against published experimental values. The goodness-of-fit is calculated using Equation (73) as follows [46]:

$$\epsilon = 1 - \frac{\sqrt{\frac{\sum_{m=1}^{N}(\tau_m - \tau_c)^2}{N-2}}}{\frac{\sum_{m=1}^{N}\tau_m}{N}}, \tag{73}$$

where τ_m represents the measured test datum, τ_c denotes the calculated result from each model and N corresponds to the number of test data points used in the comparison. The quantity ϵ is defined as the ratio of the root-mean-square error of the test results to the mean value of the published data. It serves as a statistical measure to evaluate the accuracy of the predictions obtained from each model. As ϵ approaches 1, it indicates a higher degree of conformity between the predicted results and the published data, thereby yielding a more reliable fit.

6. **Results and Discussion.** The vibration response of the system varies due to the dissimilarity in excitation forces applied to each wheel of a wheelchair-occupant system. The impact of distinct force excitations on the wheelchair-occupant motion is investigated. The equations governing the motion of the wheelchair-occupant system for each wheel in response to sinusoidal inputs are formulated, utilizing the previously obtained force excitations. As expressed in Equations (36)∼(73), the dynamic responses in terms of displacement, velocity and force result from the sinusoidal force excitations acting on the wheels. These responses arise from interactions with diverse surfaces on the floor, contributing to the overall vibrational behavior of the system.

6.1. **Validation of the 13-DOF model with varied input excitations for four wheels during movement.** This paper validates a 13-DOF model for a wheelchair-occupant system subjected to vertical vibrations from distinct input excitations at each wheel during motion. The system comprises two main subsystems: the occupant and the wheelchair. The occupant subsystem includes lumped-masses for the head, back, torso, thorax, diaphragm, abdomen and pelvis, all interconnected by linear springs and dampers. The wheelchair subsystem features lumped-masses for the seat cushion, suspension and four wheels, also interconnected by linear springs and dampers. Each wheel operates as a linear mass-spring-damper system, each with its unique displacement pattern. The wheelchair-frame is modeled as a rigid body connected to the wheels via four linear springs and dampers. Model parameters were derived from literature and experimental data.

Table 1 details the occupant parameters, including masses, damping coefficients and spring coefficients for each body segment. Table 2 lists the wheelchair parameters, such as masses, damping coefficients and spring coefficients for the seat, wheelchair-frame and

individual wheels. Additionally, Table 2 provides the vibration amplitude for each wheel, reflecting the input wave size. The input frequency considered ranges from 0.5∼11 [Hz]. The model uses a time-domain approach, applying the Newmark algorithm to solving the linear equations of motion, which is suitable for systems with variable stiffness and damping, accommodating diverse input excitations such as sinusoidal road surfaces. Figure 3 shows the model's responses concerning the head-to-pelvis acceleration ratio against input frequency and initial displacement for each wheel. The results demonstrate the model's validity and reliability, aligning well with experimental data from Patil and Palanichamy [47]. The first resonance peak occurs between 3∼5 [Hz], matching the natural vertical frequency of the human body. Figure 3 further compares the model's responses with experimental data from Patil and Palanichamy [47] under sinusoidal inputs, confirming that the model accurately captures the dynamic behavior of the wheelchair-occupant system under various input conditions. The goodness-of-fit between the simulated and experimental values is 92[%], indicating a high level of agreement. This paper establishes that the 13-DOF model is a valuable tool for predicting and evaluating the effects of vertical vibrations on wheelchair occupants. It provides significant insights into the dynamic response and vibration transmission to different body segments, considering various factors such as cushion type, input amplitude and input frequency. Moreover, the model can be utilized to design and optimize wheelchair components and accessories to improve the comfort and safety of wheelchair users.

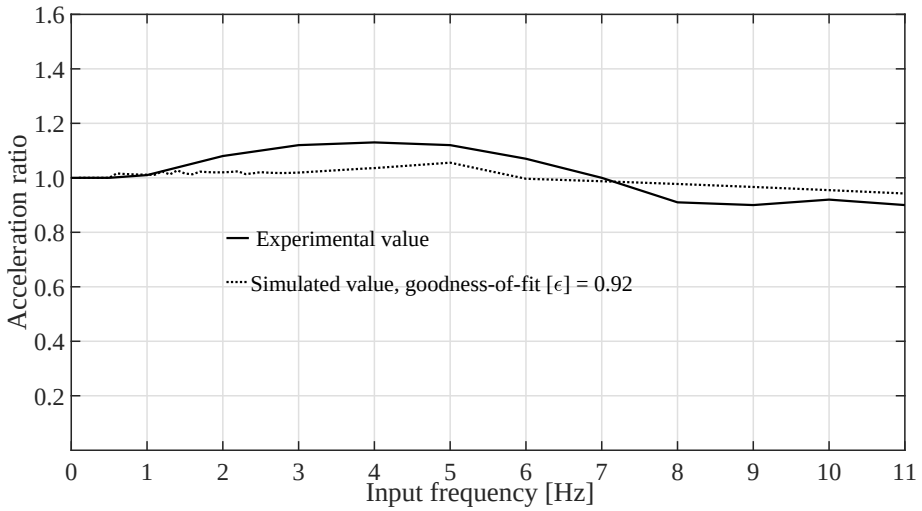

FIGURE 3. Amplitude acceleration ratios of head-to-pelvis of wheelchair occupant on foam-based cushion

Evaluating the goodness-of-fit is fundamental for validating a statistical model such as this 13-DOF model under varied input excitations for four-wheel movement. Goodness of fit is crucial in determining how well a model captures the desired data, indicative of its predictive performance. One important metric is the coefficient of determination (GOF), which represents the proportion of variance in the dependent variable that the independent variables can predict. Therefore, a GOF value of 0.92, shown in Figure 3, indicates that 92[%] of the outcome variability is accounted for by the model, demonstrating robust alignment. To augment clarity and rigor, relevant charts like those in Figure 3 should be included, which illustrate the relationship between experimental and simulated data points. Including specific numerical values, such as the GOF within these charts, provides both a visual and quantitative perspective on the model's appropriateness. Plotting

actual versus predicted values, emphasizing the experimental value line and clearly annotating the GOF value, allows for a direct comparison of model predictions against actual data points. Presenting graphs that depict simulated versus experimental values with a prominently annotated GOF of 0.92 vividly demonstrates the model's predictive accuracy. Incorporating these elements into your analysis enhances its clarity and persuasiveness, supported by specific empirical evidence, thereby strengthening its overall validity.

6.2. **Comparative analysis of body segment and seat transmissibilities in vibration.** Goodness-of-fit, a statistical measure, was utilized to evaluate the congruence between the transmissibility results derived from the computational model and empirical data obtained from real-world experiments. Figure 4 and Table 3 present empirical data from wheelchair road course (WRC) tests [10], providing specific numerical values to corroborate the model's accuracy. Figure 4 delineates the region for seat transmissibility, serving as a benchmark to evaluate the model's precision in approximating the sinusoidal patterns associated with wheelchair motion at various displacements for each wheel. The purple dashed line represents the measured transmissibility, while the orange solid line denotes the simulated seat transmissibility.

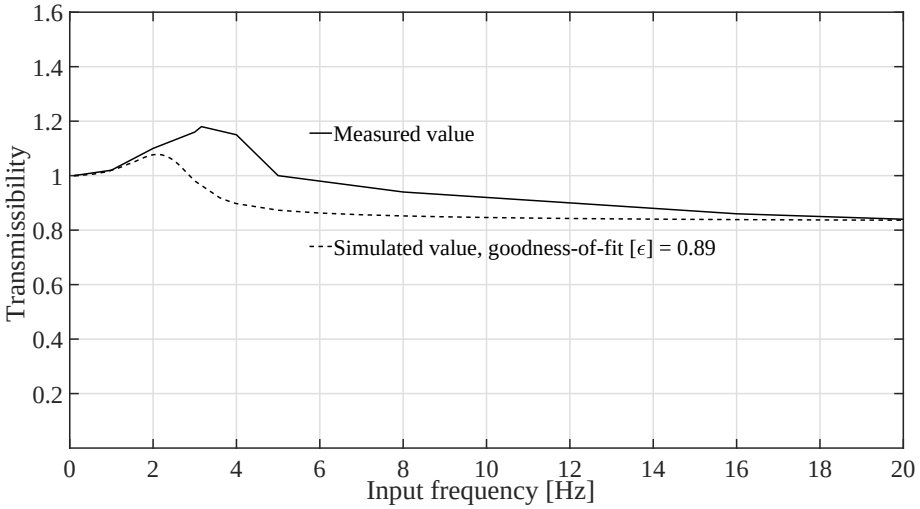

FIGURE 4. Measured and predicted amplitudes of seat transmissibility for foam-based cushion

TABLE 3. Corresponding frequency (f, [Hz]), peak transmissibility ratios (T) from actual wheelchair road course (WRC) test [10] and goodness-of-fit (ϵ) results from 13-DOF model runs

Cushion	WRC		13-DOF		
	f	T	f	T	ϵ
Foam-based	3.36	1.13	2.1	1.08	0.89

Table 3 summarizes the peak transmissibility values and their corresponding frequencies for body segments supported by foam-based cushions. The peak measurements from the WRC and 13-DOF tests are comparable, as observed in the T columns of Table 3. However, the frequencies at which these peaks occur, denoted in the f columns, show significant variance. This discrepancy likely stems from the 13-DOF model being calibrated using seat transmissibility data obtained from harmonic input excitation within

the 0.5∼20 [Hz] range, whereas the road surface-induced vibrations experienced during the WRC tests covered a broader frequency spectrum. Equation (73) was employed to assess the goodness-of-fit of the peak transmissibility values from the WRC and 13-DOF tests, with results delineated in Table 3. According to Figure 4, the model's predictions align closely with real-world results from the WRC tests, achieving a goodness-of-fit of 89[%]. This high degree of similarity underscores the model's effectiveness in replicating vibration transmissibility characteristics and highlights the utility of mathematical modeling in optimizing wheelchair cushion design.

This paper conclusively demonstrates that the 13-DOF model, utilizing the Newmark approach, surpasses alternative methods. It should be a valuable consideration for clinicians seeking to predict and mitigate the effects of whole-body vibration on wheelchair users. Integrating specific numerical values and detailed charts clarifies the model's goodness-of-fit and enhances its predictive ability, making it a powerful tool in optimizing wheelchair cushion design.

In the biodynamic assessment of the wheelchair and occupant model, extensive investigations have explored the biodynamic responses of individual human body parts to vertical vibrations, specifically focusing on transmissibility magnitudes. Mathematical models of varying complexities have been devised and thorough data collection has been undertaken to characterize these response functions under diverse experimental conditions. This paper presents data compiled using mathematical models based on well-defined assumptions. Figures 5 and 6 portray the steady-state responses of the wheelchair and various body parts to vertical vibrations within the frequency range of 0.5 to 30 [Hz]. In Figure 5, a comparison of vibration transmissibility from the excitation to the wheelchair occupant's head, back, thorax and abdomen is provided for tests conducted on a foam-based cushion. The solid lines represent the transmissibility to the head and back, while the dotted lines represent the transmissibility to the abdomen and thorax. Similarly, Figure 6 examines the vibration transmissibility from the excitation source to the wheelchair occupant's torso, diaphragm and pelvis. Here, the solid lines represent the transmissibility to the diaphragm and pelvis, while the dotted lines represent the transmissibility to the torso.

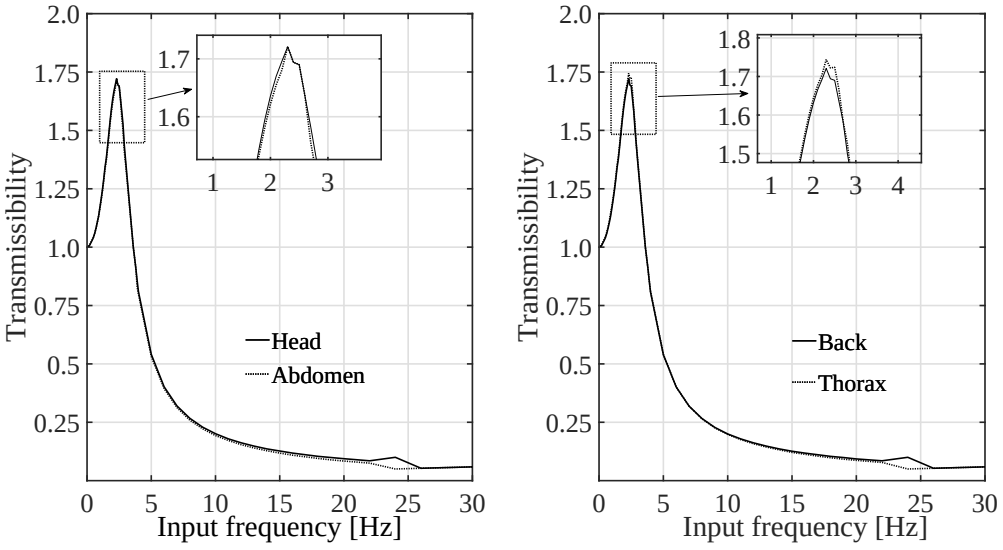

FIGURE 5. Transmissibility amplitudes of head, back, thorax and abdomen of wheelchair occupant

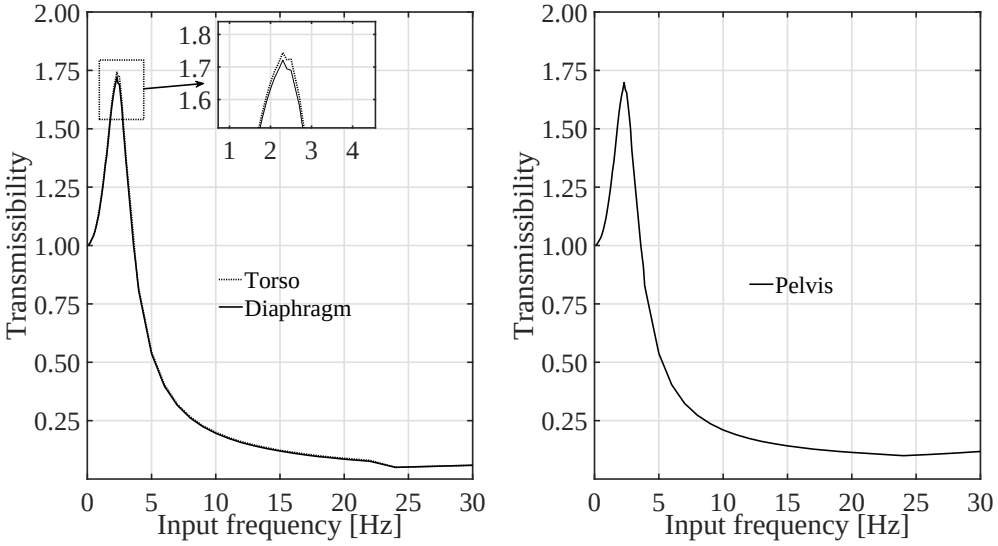

FIGURE 6. Transmissibility amplitudes of torso, diaphragm and pelvis of wheelchair occupant

TABLE 4. Summary of peak transmissibility values and corresponding frequencies for various body segments supported by foam-based cushion types

Body segment	Frequency f [Hz]	Transmissibility T
Torso	2.3	1.722
Pelvis	2.3	1.675
Head	2.3	1.704
Back	2.3	1.701
Thorax	2.3	1.713
Diaphragm	2.3	1.702
Abdomen	2.3	1.689

The simulation results of transmissibilities for various body segments, supported by foam-based cushion types, are depicted in Figures 5 and 6 and summarized in Table 4. The torso experienced the highest shock of 1.722 at 2.3 [Hz], while the pelvis had the lowest shock of 1.675 at the same frequency on the foam-based pad. The maximum magnitude for all mass segments occurred at the common frequency of 2.3 [Hz]. The model's response in this paper underscores that cushion parameters are crucial for characterizing vibration and should be considered in the engineering of the wheelchair seat to enhance ride comfort.

The model in this paper revealed resonance frequencies and absolute maximum acceleration ratios, as illustrated in Figures 5 and 6. Notably, the torso exhibited a transmissibility of 1.722 at 2.3 [Hz], while the wheelchair seat demonstrated a maximum amplitude of 1.08 at 2.1 [Hz], as shown in Figure 4 and Table 3. In comparison, the body as a whole exhibited higher responses than the wheelchair seat and the response of the head was consistent with the experimental findings reported by [20, 34, 35]. For the head, equipped with a suspension system, the response registered at 1.704. Regarding the back, torso, thorax, diaphragm, abdomen and pelvis, their responses were measured as 1.701, 1.722, 1.713, 1.702, 1.689 and 1.675, respectively, all at 2.3 [Hz]. Remarkably, for the model solved by the Newmark method with a seat cushion, it was found that the goodness-of-fit was 89[%] when the wheelchair moved under different input harmonic forces for each of

the four wheels. At higher frequencies (5∼30 [Hz]), the average response of all body parts was observed to be on the order of 0.28.

6.3. **Biodynamic assessment of wheelchair and occupant model.** This paper utilized a thoroughly validated composite model with minimal response parameters to explore the acceleration responses of different body segments under vertical sinusoidal vibrations. The findings unveiled unique response characteristics and sensitivities of various body parts to transmitted vibrations, offering valuable insights into the effects of vibrations on human well-being and performance. The study highlighted the efficacy of foam-based seat cushions and suspension systems in significantly improving driving comfort. This improvement was achieved by notably decreasing acceleration responses within the 5∼30 [Hz] frequency range while ensuring that response levels stayed within the exposure limitations outlined by ISO standards [44, 47]. These discoveries make substantial contributions to the advancement of ergonomic systems and deepen our knowledge of vibration transmission concerning human health and comfort.

Figures 7 and 8 compare acceleration vibrations in different body segments such as the head, torso, diaphragm and pelvis against the exposure limit curves specified by ISO 2631-1:1997 for durations of 16 minutes, 25 minutes and 1 hour. Solid lines represent the acceleration responses of the head and pelvis, while dotted lines represent the responses of the diaphragm and torso. Likewise, Figure 8 contrasts acceleration vibrations affecting the back and wheelchair-frame, the thorax and seat cushion and the abdomen. The interpretations of the solid and dotted lines align with Figure 7, with exposure limit curves color-coded accordingly. These figures vividly depict the influence of excitation on the comfort and safety of wheelchair users. The extensive analysis presented in Figures 7 and 8 offers crucial insights into acceleration responses during wheelchair motion. It was observed that the pelvis, seat cushion and wheelchair-frame exhibited the highest responses, reaching values of 5.4867, 51.597 and 61.8713 [m/s^2], respectively, at a frequency of 30 [Hz]. Other body segments exhibited lower responses ranging from 3.184 to 3.91 [m/s^2] at the same frequency. Importantly, all acceleration responses remained below the exposure limit curves, indicating enhanced ride comfort due to the effective

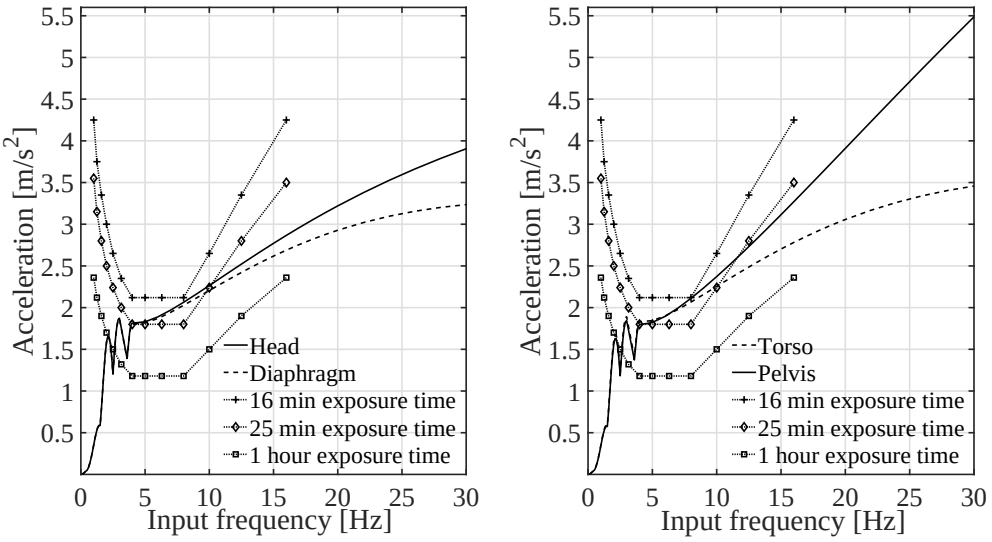

FIGURE 7. Acceleration responses of head, diaphragm, torso and pelvis of wheelchair occupant for foam-based cushion tests with ISO 2631-1:1997 exposure limit curves

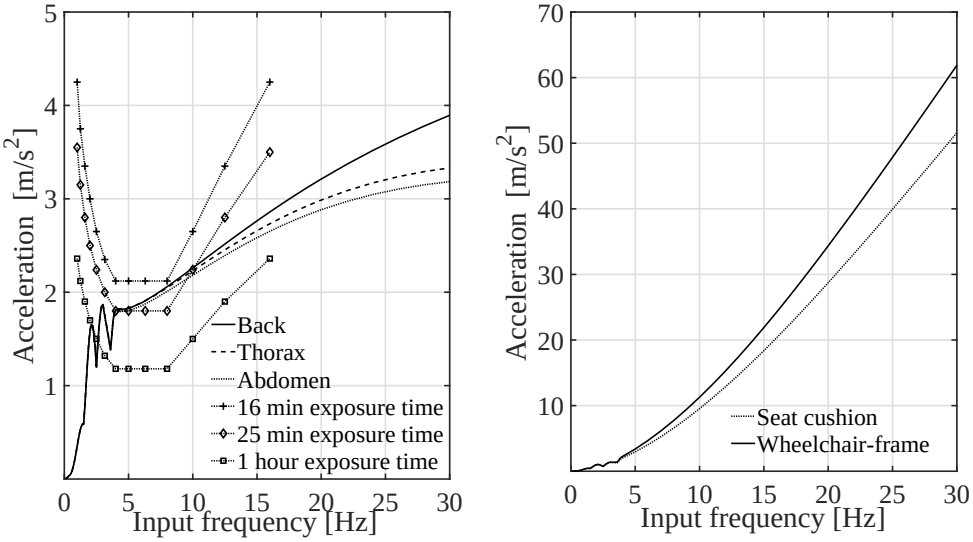

FIGURE 8. Acceleration responses of back, thorax, abdomen, wheelchair-frame and seat cushion of wheelchair occupant for foam-based cushion tests with ISO 2631-1:1997 exposure limit curves

attenuation of transmitted vibrations by the seat cushion. The frequency response of all body parts, the seat cushion and the wheelchair-frame peaked at 30 [Hz], as illustrated in Figures 7 and 8. An evaluation of acceleration responses across various body segments during wheelchair motion was presented, stressing compliance with the exposure limit curves defined by ISO. The graphs exhibit consistent adherence to acceleration responses below the 16-minute exposure limit curve, showcasing the wheelchair design's capability to effectively mitigate vibrations. The pelvis, in particular, consistently maintained acceleration responses within the critical frequency band of 0.5∼30 [Hz], all below the stringent 16-minute exposure limit curve [44, 47]. This conformity ensures that discomfort and fatigue levels remain within acceptable thresholds. Additionally, all body parts consistently showcased acceleration responses below the 25-minute exposure limit curve. For vertical vibrations, accelerations ranged from 0 to 1.64 [m/s^2] in the 0.5∼4 [Hz] frequency band and exceeded 2 [m/s^2] beyond 4 [Hz]. The simulated values consistently stayed below the specified curves, signifying adherence to acceptable exposure limits and a commitment to enhancing ride comfort for wheelchair users. However, in the frequency range surpassing 4∼10 [Hz], surpassing the exposure limit curve indicated unacceptable exposure levels, highlighting discomfort and potential health risks. Additionally, the 1-hour exposure limit curve outlined acceleration levels ranging from 0 to 1.8 [m/s^2] in the 0.5∼2 [Hz] frequency band. Remaining below this curve mitigates the risk of health implications, confirming the effectiveness of the new seat and wheelchair-frame in significantly improving ride comfort. Table 5 presents the absolute response amplitudes of displacement (y in [m]), acceleration ($\ddot{y}$ in [m/s^2]) and transmissibility (T) for various body parts in foam-based cushion tests. The outcomes highlight significant impacts of foam-based cushions on the dynamic responses of different body segments. Displacement amplitudes for all body parts ranged from 0.009995∼0.01028 [m], with the torso exhibiting the highest value and the pelvis the lowest. These values aligned with the ISO 2631-1:1997 standard for human exposure to whole-body vibration, indicating consistent support and damping provided by the foam-based cushion across body parts. Acceleration amplitudes varied between 3.184 [m/s^2] and 5.4867 [m/s^2], with the pelvis registering the highest and the

TABLE 5. Displacement (y in [m]), acceleration ($\ddot{y}$ in [m/s^2]) and transmissibility (T), response of different body parts in foam-based cushion test

Body parts	Absolute amplitude		
	Displacement ($y_{1\text{-}7}$, [m])	Acceleration ($\ddot{y}_{1\text{-}7}$, [m^2/s])	Transmissibilities ($T_{1\text{-}7}$)
Head	$y_1 = 0.01017$	$\ddot{y}_1 = 3.9051$	$T_1 = 1.704$
Back	$y_2 = 0.01015$	$\ddot{y}_2 = 3.8944$	$T_2 = 1.701$
Torso	$y_3 = 0.01028$	$\ddot{y}_3 = 3.4579$	$T_3 = 1.722$
Thorax	$y_4 = 0.01023$	$\ddot{y}_4 = 3.3312$	$T_4 = 1.713$
Diaphragm	$y_5 = 0.01016$	$\ddot{y}_5 = 3.2353$	$T_5 = 1.702$
Abdomen	$y_6 = 0.01009$	$\ddot{y}_6 = 3.184$	$T_6 = 1.689$
Pelvis	$y_7 = 0.009995$	$\ddot{y}_7 = 5.4867$	$T_7 = 1.675$

abdomen the lowest acceleration values. These values exceeded the ISO standard, suggesting ineffective vibration reduction by the cushion and potential negative health impacts. Transmissibility values ranged from 1.675∼1.722, with the torso showing the highest and the pelvis the lowest. These values surpassing unity imply an increase in vibration rather than mitigation, likely due to resonance phenomena.

7. **Conclusion.** This paper introduced a sophisticated 13-degree-of-freedom (DOF) model for a wheelchair-occupant system meticulously engineered to replicate vertical vibrations induced by various input excitations at each wheel during motion. Demonstrating exceptional reliability and precision, the model achieved goodness-of-fit scores of 92[%] for validation and 89[%] for the WRC test. Employing a time-domain approach, the Newmark algorithm was utilized to solve the linear equations of motion and deftly transitioned to the frequency domain via Fourier transform. This comprehensive validation, which involved comparing simulated outcomes with data from previous studies, facilitated an in-depth exploration of biodynamic responses and vibration transmission to various body parts and wheelchair components under diverse input scenarios and exposure durations. The evaluation against ISO 2631-1:1997 exposure limit curves yielded significant insights into the comfort and safety of wheelchair users. The paper revealed that the pelvis, seat cushion and wheelchair-frame exhibited pronounced acceleration responses, whereas other body parts showed comparatively subdued responses. Transmissibility values near or exceeding 1 indicated substantial vibration transmission within the system, with foam-based cushions and suspensions proving less effective at attenuating higher frequency vibrations. Notably, acceleration responses for all body parts remained consistently below the exposure limit curves across all durations, underscoring the enhanced ride comfort provided by the novel seat and wheelchair-frame system.

The 13-DOF model emerged as an indispensable predictive tool for evaluating the impact of vertical vibrations on wheelchair occupants, underscoring the critical role of precise engineering in seat cushions and wheelchair-frame systems in significantly enhancing ride comfort and mitigating health risks. This marks a substantial advancement in wheelchair ergonomics. Future research directions in wheelchair ergonomics include expanding the model to encompass diverse types of vibrations and exploring adaptive control strategies tailored to optimize user comfort and safety through personalized adjustments in seat cushion and suspension parameters based on individual preferences and vibration inputs. Recognizing the model's limitations remains essential for a holistic understanding of its scope and practical applicability, despite its success in assessing vertical vibrations induced

by various wheel inputs and its commendable validation goodness-of-fit scores for the WRC test. These limitations include the generalization of foam-based cushion impacts and the complexities of non-linear system interactions. Addressing these limitations and enhancing the model's precision are crucial steps towards leveraging its full potential in diverse practical scenarios. Future research endeavors, including the examination of alternative vibration types beyond vertical vibrations and the implementation of adaptive control strategies to optimize user comfort, promise to bolster the model's robustness and relevance in dynamic settings. Providing valuable insights and practical recommendations for improving wheelchair design, the comprehensive findings from this paper emphasize the importance of thoughtful engineering in enhancing user comfort and safety. Through continued research and development, the 13-DOF model will serve as a foundational tool in advancing the field of wheelchair ergonomics, contributing to an improved quality of life for wheelchair users.

Acknowledgment. This material is the result of work supported by JSPS KAKENHI Grant Number JP21K03930.

REFERENCES

[1] M. L. Toro-Hernández, L. Alvarez, M. C. Vargas-Chaparro and M. Goldberg, Final year students' knowledge on basic manual wheelchair provision: The state of occupational therapy programs in Colombia, *Occupation Therapy International*, vol.2020, pp.1-8, Article ID 3025456, 2020.

[2] A. M. Geers, E. C. Prinsen, D. J. van der Pijl, A. Bergsma, J. S. Rietman and B. F. J. M. Koopman, Head support in wheelchairs (scoping review): State-of-the-art and beyond, *Disability and Rehabilitation: Assistive Technology*, DOI: 10.1080/17483107.2021.1892840, 2021.

[3] O. Lariviere, D. Chadefaux, C. Sauret and P. Thoreux, Vibration response of manual wheelchairs according to loads, propulsion methods, speeds and ground floor types, *Vibration*, vol.6, pp.762-776, 2023.

[4] ISO 8608:2016, *Mechanical Vibration – Road Surface Profiles – Reporting of Measured Data*, ISO, Geneva, Switzerland, 2016.

[5] M. Agostinacchio, D. Ciampa and S. Olita, Road pavement surface irregularities induced vibrations – A Matlab® approach, *European Transport Research Review*, vol.6, pp.267-275, 2014.

[6] J. D. Quadros, P. Suhas and N. L. Vaishak, Ideal operating speed for a two-wheeler rider on varying terrain amplitudes – A numerical study, *Journal of Mechanical Science and Technology*, vol.30, pp.2435-2442, 2016.

[7] M. J. Griffin, Discomfort from feeling vehicle vibration, *Vehicle System Dynamics*, vol.45, pp.679-688, 2007.

[8] E. Wolf, J. Pearlman, M. L. Boninger and R. A. Cooper, Health risks of vibration exposure to wheelchair users in the community, *Journal of Spinal Cord Medicine*, vol.31, pp.361-369, 2008.

[9] T. Waga, S. Ura, M. Nagamori, H. Uchiyama and A. Shionoya, Influence of material on wheelchair vibrations, *The 13th Conference International Sports Engineering Association*, pp.1-6, 2020.

[10] Y. Garcia-Mendez, J. L. Pearlman, M. L. Boninger and R. A. Cooper, Health risks of vibration exposure to wheelchair users in the community, *Journal of Spinal Cord Medicine*, vol.36, pp.365-375, 2013.

[11] J. Duvall, R. Cooper, E. Sinagra, D. Stuckey, J. Brown and J. Pearlman, Development of surface roughness standards for pathways used by wheelchairs, *Transportation Research Record*, pp.149-156, 2013.

[12] J. Duvall, E. Sinagra, R. Cooper and J. Pearlman, Proposed pedestrian pathway roughness thresholds to ensure safety and comfort for wheelchair users, *Assistive Technology*, vol.28, pp.209-215, 2016.

[13] M. Hischke and R. F. Reiser, Effect of rear wheel suspension on tilt-in-space wheelchair shock and vibration attenuation, *Physical Medicine & Rehabilitation*, vol.10, pp.1040-1050, 2018.

[14] S. A. Adam, N. A. A. Jalil, K. A. M. Rezali and Y. G. Ng, The effect of posture and vibration magnitude on the vertical vibration transmissibility of tractor suspension system, *International Journal of Industrial Ergonomics*, vol.80, DOI: 10.1016/j.ergon.2020.103014, 2020.

[15] K. Brown, H. Flashner, J. McNitt-Gray and P. Requejo, Modeling wheelchair-users undergoing vibrations, *Journal of Biomechanical Engineering*, vol.139, DOI: 10.1115/1.4037220, 2017.

[16] P. Weerapong, K. Hashikura, M. A. S. Kamal, I. Murakami and K. Yamada, Analysis of model output in the simulation of a wheelchair-occupant system subjected to vibration, *ICIC Express Letters, Part B: Applications*, vol.14, no.4, pp.389-398, 2023.

[17] Y. Garcia-Mendez, J. Pearlman, M. L. Boninger and R. A. Cooper, Whole-body vibration exposure in manual wheelchair users: Influence of wheelchair components, *Medical Engineering & Physics*, vol.52, pp.1-7, 2018.

[18] V. Nadalin, N. Kreiger, M. E. Parent, A. Salmoni, K. Sass-Kortsak, J. Siemiatycki, M. Sloan and J. Purdham, Prostate cancer and occupational whole-body vibration exposure, *Annals of Occupational Hygiene*, vol.56, pp.968-974, 2012.

[19] O. Larivière, D. Chadefaux, C. Sauret and P. Thoreux, Vibration transmission during manual wheelchair propulsion: A systematic review, *Vibration*, vol.4, pp.444-481, 2021.

[20] P. Weerapong, M. Katahira, K. Hashikura, M. A. S. Kamal, I. Murakami and K. Yamada, Modal analysis for evaluating the transmission of vertical vibrations in a wheelchair-occupant model with foam-based seat cushion, *International Journal of Innovative Computing, Information and Control*, vol.19, no.6, pp.1933-1952, 2023.

[21] O. Lariviere, D. Chadefaux, C. Sauret and P. Thoreux, Experimental modal analysis of a standard wheelchair: A preliminary study, *Computer Methods in Biomechanics and Biomedical Engineering*, vol.23, pp.164-165, 2020.

[22] O. Lariviere, D. Chadefaux, C. Sauret, L. Kordulas and P. Thoreux, Modal characterization of manual wheelchairs, *Vibration*, vol.5, pp.442-463, 2022.

[23] N. F. Nangolo, J. Soukup, L. Rychlíková and J. Skocilas, A combined numerical and modal analysis on vertical vibration response of railway vehicle, *Procedia Engineering*, vol.96, pp.310-319, 2014.

[24] J. Schwochow and G. Jelcic, Automatic operational modal analysis for aeroelastic applications, *Proc. of the 6th International Operational Modal Analysis Conference*, pp.1-14, 2015.

[25] J. C. Miao, P. Zhu, G. L. Shi and G. L. Chen, Study on sub-cycling for flexible multi-body dynamics based on Newmark method, *International Journal for Numerical Methods in Engineering*, vol.75, pp.188-211, 2008.

[26] J. Yuan, J. Li, W. Wei and P. Liu, Operational modal identification of ultra-precision fly-cutting machine tools based on least-squares complex frequency-domain method, *International Journal of Advanced Manufacturing Technology*, vol.119, pp.1-10, 2022.

[27] P. Weerapong, M. Katahira, K. Kaewkongtham, W. Sudsomboon, C. Kaewdee, W. Pansrinual, N. T. Mai, K. Hashikura, M. A. S. Kamal, I. Murakami and K. Yamada, A state-space approach to analyzing vertical vibration behavior in wheelchair-occupant systems with a composite model, *International Journal of Innovative Computing, Information and Control*, vol.20, no.2, pp.437-460, 2024.

[28] F. Chénier and R. Aissaoui, Effect of wheelchair frame material on users' mechanical work and transmitted vibration, *BioMed Research International*, vol.2014, pp.1-12, 2014.

[29] Y. S. Kim, K. Suzuki and S. J. Hong, Product redesign for service considerations using affordances for service activities, *Sustainability*, vol.12, pp.1-20, 2020.

[30] M. Lalumiere, G. Desroches, P. Gourdou, F. Routhier, L. Bouyer and D. H. Gagnon, Manual wheelchair users gradually face fewer postural stability and control challenges with increasing rolling resistance while maintaining a rear-wheel wheelie, *Human Movement Science*, vol.62, pp.194-201, 2018.

[31] G. Chwalik-Pilszyk, D. Ziemianski and M. S. Kozien, Experimental investigations on transmission of whole body vibration to the wheelchair user's body, *Open Engineering*, vol.12, pp.431-438, 2022.

[32] A. Asgharnia, H. Schwartz and M. Atia, Learning multi-objective deception in a two-player differential game using reinforcement learning and multi-objective genetic algorithm, *International Journal of Innovative Computing, Information and Control*, vol.18, no.6, pp.1667-1688, 2022.

[33] Y. Garcia-Mendez, J. L. Pearlman, R. A. Cooper and M. L. Boninger, Dynamic stiffness and transmissibility of commercially available wheelchair cushions using a laboratory test method, *Journal of Rehabilitation Research and Development*, vol.49, pp.7-22, 2012.

[34] P. Weerapong, K. Hashikura, M. A. S. Kamal, I. Murakam and K. Yamada, Simulated response analysis: Modelling a wheelchair-occupant system subjected to vibration, *International Journal of Innovative Computing, Information and Control*, vol.19, no.2, pp.307-323, 2023.

[35] P. Weerapong, K. Hashikura, M. A. S. Kamal and K. Yamada, A biodynamic model of wheelchair with changeable seat cushions subjected to vertical vibrations, *ICIC Express Letters*, vol.16, no.1, pp.33-41, 2022.

[36] S. Y. Chang, Y. C. Huang and C. H. Wang, Analysis of Newmark explicit integration method for nonlinear systems, *Journal of Mechanics*, vol.22, pp.321-329, 2006.
[37] Ş. Yavuz, L. Malgaca and H. Karagülle, Analysis of active vibration control of multi-degree-of-freedom flexible systems by Newmark method, *Simulation Modelling Practice and Theory*, vol.69, pp.136-148, 2016.
[38] S. Pourzeynali, X. Zhu, A. G. Zadeh, M. Rashidi and B. Samali, Simultaneous identification of bridge structural damage and moving loads using the explicit form of Newmark-β method: Numerical and experimental studies, *Remote Sensing*, vol.14, DOI: 10.3390/rs14010119, 2022.
[39] D. Liu, B. Liu, X. Li and K. Shi, Theoretical and numerical examination of a novel method for identifying bridge moving force using an instrumented vehicle, *Buildings*, vol.13, DOI: 10.3390/buildings13061481, 2023.
[40] N. M. Newmark, A method of computation for structural dynamics, *Journal of Engineering Mechanics Division*, vol.85, pp.67-94, 1959.
[41] A. Ramos, P. Talaia and F. J. Q. de Melo, Pseudo-dynamic analysis of a cemented hip arthroplasty using a force method based on the Newmark algorithm, *Computer Methods in Biomechanics and Biomedical Engineering*, vol.19, pp.49-59, 2016.
[42] S. Pourzeynali, X. Zhu, A. G. Zadeh, M. Rashidi and B. Samali, Comprehensive study of moving load identification on bridge structures using the explicit form of Newmark-β method: Numerical and experimental studies, *Remote Sensing*, vol.13, pp.1-26, 2021.
[43] L. Wang, J. Zhang, X. Huang and G. Tan, Study on the dynamic stability and spectral characteristics of a toppling dangerous rock mass under seismic excitation, *Sustainability*, vol.15, DOI: 10.3390/su152115397, 2023.
[44] ISO 2631-1:1997, *Mechanical Vibration and Shock-Evaluation of Human Exposure to Whole-Body Vibration*, ISO, Geneva, Switzerland, 1997.
[45] H. Cao, Y. Lu and D. Chen, Analysis of vehicle-bridge coupling vibration characteristics of curved girder bridges, *Applied Sciences*, vol.14, DOI: 10.3390/app14052021, 2024.
[46] C. C. Liang and C. F. Chiang, A study on biodynamic models of seated human subjects exposed to vertical vibration, *International Journal of Industrial Ergonomics*, vol.36, pp.869-890, 2006.
[47] M. K. Patil and M. S. Palanichamy, A mathematical model of tractor-occupant system with a new seat suspension for minimization of vibration response, *Applied Mathematical Modelling*, vol.12, pp.63-71, 1988.
[48] M. F. Hikmawan and A. S. Nugraha, Analysis of electric wheelchair passenger comfort with a half car model approach, *2016 International Conference on Sustainable Energy Engineering and Application (ICSEEA)*, pp.76-80, 2016.
[49] Q. Li, D. Zuo, Y. Feng and D. Wen, Research on high-performance Fourier transform algorithms based on the NPU, *Applied Sciences*, vol.14, pp.1-19, 2024.
[50] W. Qi, D. Pan, Y. Gao, W. Lu and Y. Huang, A fast frequency domain method for steady-state solution of forced vibration of system with complex damping, *Applied Sciences*, vol.10, pp.1-13, 2020.

Author Biography

Pongtep Weerapong received his B.E. and M.E. degrees in Materials Engineering and Polymer Processing Engineering, respectively, from King Mongkut's University of Technology Thonburi (KMUTT), Thailand. He obtained his Ph.D. in Mechanical Science and Technology from Gunma University, Japan, in 2023. He is currently a full-time professor at the Faculty of Industrial Technology at Nakhon Si Thammarat Rajabhat University, Thailand. His current research interests include assistive technology for children with disabilities and whole-body vibration.

Kreetha Kaewkongtham received the B.E. degree in Materials Handling Technology in 2000 and the B.Ind.Tech degree in Mechanical Technology in 2009 from King Mongkut's University of Technology North Bangkok (KMUTNB), Thailand. He is currently a full-time professor at the Faculty of Industrial Technology at Nakhon Si Thammarat Rajabhat University, Thailand. His research interests include assistive technology, pneumatic systems and whole-body vibration.

Narapong Chuaychai received the B.Ind.Tech degree in Welding Technology from King Mongkut's University of Technology North Bangkok, Thailand, in 2000. He obtained the Master of Education (Industrial Technology) from Nakhon Si Thammarat Rajabhat University, Thailand, in 2012 and his Ph.D. from Phranakhon Rajabhat University, Thailand, in 2019. He is currently a full-time professor at the Faculty of Industrial Technology at Nakhon Si Thammarat Rajabhat University, Thailand. His research interests include welding technology, and wheelchair technology.

Suppharerk Kathammanee received his B.Sc. degree in Ceramic Technology from the Faculty of Industrial Technology at Nakhon Si Thammarat Rajabhat University, Thailand, in 2001. He obtained his M.Sc. degree in Industrial and Organizational Psychology from the Faculty of Graduate Studies at Krirk University, Thailand, in 2004 and his Ph.D. from Phranakhon Rajabhat University, Thailand, in 2020. He is currently a full-time professor in the Faculty of Industrial Technology at Nakhon Si Thammarat Rajabhat University, Thailand. His research interests include ceramics technology management, industrial technology and whole-body vibration.

Weeraphol Pansrinual received the B.Sc. degree in Industrial Technology (Electronics) from Rajabhat Institute Phanakhonsriayuttaya and M.Ed. degree in Industrial Technology (Electronics) and Ph.D. in Technology Management from Phranakhon Rajabhat University, Thailand, in 2010. He is currently a full-time professor of Faculty of Industrial Technology at Nakhon Si Thammarat Rajabhat University, Thailand. His research interests include mechanical engineering education and vocational and technical education administration.

Kridtharit Thongsin received the B.Ed. degree in Industrial Technician (Building Construction) from Suan Sunandha Rajabhat University and the M.Ed. degree in Industrial Technology and Ph.D. in Technology Management from Phranakhon Rajabhat University, Thailand. He is currently a full-time professor in the Faculty of Engineering and Industrial Technology at Bansomdejchaopraya Rajabhat University, Thailand. His research interests include construction engineering education, concrete technology and machine design.

Nghia Thi Mai received the B.S., M.S. and Dr. Eng. degrees from Gunma University, Gunma, Japan in 2009, 2011 and 2014, respectively. From 2014 to 2015, she was with the Human Resources Cultivation Center, Gunma University, Gunma, Japan as a research associate. From 2015 to 2021, she worked on research on damping control for automobiles at Exedy Co., Ltd. Since 2022, she has been working as a lecturer at the Faculty of Electronics Engineering 1, Posts and Telecommunications Institute of Technology (PTIT). In addition, she is currently working as a visiting associate professor and part-time lecturer at the Department of Electronics and Mechanical Engineering, Gunma University. Her research interest includes Smith predictor, internal model control and robotics.

Md Abdus Samad Kamal received the B.Sc. degree in Electrical and Electronic Engineering from Khulna University of Engineering and Technology (KUET), Khulna, Bangladesh in 1997; Master and Doctor degrees from Kyushu University from Graduate School of Information Science and Electrical Engineering, Japan in 2003 and 2006, respectively. He was a post-doctoral fellow in Kyushu University till November 2006. He is currently an associate professor at Division of Mechanical Science and Technology, Gunma University, Japan. His current research interests are reinforcement learning, intelligent transportation systems and multiagent systems. He is a member of IEEE and SICE.

Iwanori Murakami received the B.E., M.E. and Dr. Eng. degrees from Gunma University, Kiryu City, Japan, in 1992, 1994 and 1997, respectively. He is currently an associate professor at Division of Mechanical Science and Technology, Gunma University, Japan. His research interests include control problems in the mechanical fields and robotics.

Kou Yamada received B.S. and M.S. degrees in Electrical and Information Engineering from Yamagata University, Yamagata, Japan, 1987 and 1989, respectively; and the Dr. Eng. degree from Osaka University, Osaka, Japan in 1997. He is currently a full-time professor at Division of Mechanical Science and Technology, Gunma University, Japan. His research interests include robust control, repetitive control, process control and control theory for inverse systems and infinite-dimensional systems. Prof. Yamada received the 2005 Yokoyama Award in Science and Technology, the 2005 Electrical Engineering/Electronics, Computer, Telecommunication and Information Technology International Conference (ECTI-CON2005) Best Paper Award, the Japanese Ergonomics Society Encouragement Award for Academic Paper in 2007, the 2008 Electrical Engineering/Electronics, Computer, Telecommunication and Information Technology International Conference (ECTI-CON2008) Best Paper Award and 4th International Conference on Innovative Computing, Information and Control Best Paper Award in 2009, the 14th International Conference on Innovative Computing, Information and Control Best Paper Award in 2019, Outstanding Achievement Award from Kanto Branch of Japanese Society for Engineering Education in 2022 and JSME (The Japan Society of Mechanical Engineers) Education Award in 2023. He is a member of IEEE and SICE and a fellow of JSME.